Energy landscapes of some model glass formers

Thomas F. Middleton and David J. Wales
University Chemical Laboratories, Lensfield Road, Cambridge CB2 1EW, United Kingdom
(Received 7 April 2000; revised manuscript received 26 January 2001; published 22 June 2001)

The potential energy surfaces of several model atomic glass formers have been studied using eigenvector-following techniques. Barrier distributions, cooperativity indices, path lengths, and vibrational densities of states (VDOS) are presented based upon data sets containing more than 250 000 pathways in total. We find that rearrangements can usefully be separated into ''nondiffusive'' processes, which do not change the nearest-neighbor contacts and ''diffusive'' processes, which do. We suggest a criterion to separate these classes: nondiffusive processes are those in which no atoms move more than a threshold distance. Energy barriers for the two classes of rearrangement differ much more in the ''strong'' system (Stillinger-Weber silicon) than in the ''fragile'' Lennard-Jones systems. Our results indicate that the system is not trapped in a single local minimum below the glass transition temperature, because there are numerous ''nondiffusive'' rearrangements with low barriers still accessible. Disconnectivity graphs for low-energy regions of the potential energy surface illustrate how the crystal is rapidly located once a critical nucleus is present. Finally, the calculated VDOS show a pronounced excess over the Debye density of states in the low-frequency region. Transition state searches following the eigenvectors corresponding to these soft modes converge to low-lying transition states, including some that separate nearly degenerate minima. This result provides support for the hypothesis that two-level systems and the boson peak are related.

DOI: 10.1103/PhysRevB.64.024205 PACS number(s): 61.43.Fs, 64.70.Pf, 82.20.Wt

I. INTRODUCTION

In 1969 Goldstein[1] realized that the behavior of glass formers at low temperature is a consequence of the form of the potential energy surface (PES). In the ''landscape dominated'' regime, the dynamical behavior takes place on two distinct time scales: fast intrawell oscillations and slow jumps over energy barriers between local minima on the $3N+1$-dimensional PES. This picture is applicable at temperatures where the two time scales are distinct. Somewhere above this point, the liquid is so fluid that the system does not have time to equilibrate within individual minima. This is the regime where other approaches such as mode-coupling theory[2] have been applied successfully.

The transport properties of many glass forming materials depart from the Arrhenius law $\exp(-A/RT)$. Empirically, it is found that properties such as the viscosity can be better modeled by the Vogel-Tammann-Fulcher[3–5] (VTF) equation

$$\eta = \eta_0 \exp[A/(T-T_0)], \tag{1}$$

where A is a constant and T_0 is a nonzero temperature at which the viscosity diverges. Angell has developed the strong/fragile classification scheme based largely on the VTF equation for glass forming liquids.[6] The ''fragility'' in this context is defined as the degree to which the viscosity departs from Arrhenius behavior. Strong liquids tend to have open network structures that resist structural change as a function of temperature, while fragile liquids usually have less directional interactions, such as Coulomb or Van der Waals. The behavior of the viscosity is found to correlate with other properties of the material: the thermodynamic properties of strong liquids tend to change smoothly at the glass transition, which is often defined as the point at which the viscosity reaches 10^{13} poise. Fragile liquids tend to exhibit a large jump in the heat capacity at a clearly defined glass transition, a feature that Angell has associated with a higher density of minima on the energy landscape per unit energy increase, with low barriers between them.[7] In recent years, it has proved possible to relate the dynamics and thermodynamics of finite systems to the underlying PES in some detail,[8] and the same approach should help to develop the connections proposed for glasses in a quantitative manner.

Angell has also pointed out that a liquid can be strong or fragile depending on its density or the conditions under which it was prepared.[7] Analysis of stationary points in monatomic glasses and silica has shown that increased pressure generally lowers the barriers between minima and can eventually destabilize them.[9,10] Clearly the PES is also a function of pressure or volume, and in the present work constant volume conditions are used throughout, including two different volumes (densities) for one of the systems.

Kauzmann noted that the extrapolated excess entropy of a number of supercooled liquids vanishes at finite temperature somewhere below the glass transition.[11] This isoentropy temperature, now known as the Kauzmann temperature T_K, correlates well with the VTF divergence temperature T_0, and it has been suggested that $T_0 \equiv T_K$, and that they correspond to the configurational ground-state temperature.[6]

In the longer-time regime, in which transitions between separate minima occur, the relaxation functions are often well modeled by the Kohlrausch-Williams-Watts stretched exponential relaxation function $\exp[-(t/\tau)^{\theta}]$, $0<\theta\leqslant 1$.[12] Conventional exponential Debye relaxation corresponds to $\theta=1$. Fragile liquids tend to depart from Debye behavior and θ is generally found to decrease with increasing fragility. Palmer *et al.* found that this type of stretched exponential function can arise from a model with hierarchically constrained dynamics, where some transition states may only be

 ©2001 The American Physical Society

accessed once others have been overcome.[13] Thus slower degrees of freedom constrain faster ones, generating a wide range of relaxation times.

From measurements of dielectric relaxation, Johari and Goldstein found that there existed a bifurcation in relaxation times.[14] In fragile liquids there are generally two dominant relaxation processes: faster β processes and slower non-Arrhenius α processes. (The β processes discussed here are sometimes referred to as ''slow'' β processes to distinguish them from the ''fast'' β processes of mode-coupling theory.) As the temperature increases, these two relaxation ''processes'' become indistinguishable. In strong liquids, this bifurcation tends not to be seen, and only β processes with an Arrhenius-type temperature dependence are observed.

Stillinger has suggested[15] that Johari-Goldstein β processes[14] involve a transition between two minima involving a single transition state, while α processes are a concerted series of such transitions, taking the configuration point from one ''megabasin'' or ''crater'' to another. The large energies and entropies of activation for these processes might then cause them to be frozen out at a relatively higher temperature than the β processes. This is a similar concept to the idea of multiple funnels—sets of minima linked by kinetically convergent pathways to a common lowest-energy structure[16]—that have been found to be features in the energy landscapes of various systems.[8,17] If Stillinger's suggestion is correct, then the distribution of barriers between pairs of minima must be similar throughout the relevant parts of the PES explored, as β processes have Arrhenius temperature dependence. Strong liquids do not exhibit the α-β bifurcation, so a possible corollary of Stillinger's idea is that strong liquids have a ''uniformly rough'' potential energy landscape, whereas fragile liquids have local minima arranged into megabasins. However, the present results suggest a somewhat different interpretation.

Another characteristic property of glasses is the ''boson peak.'' At low frequency, the density of states $g(\omega)$ is assumed to be proportional to ω^2 in Debye theory. The boson peak is visible as an excess in $g(\omega)$ at low frequency ($\nu \sim 1$ THz) over that predicted by Debye theory. This phenomenon has been observed with a number of experimental techniques, including neutron scattering[18] and Raman spectroscopy[19] and is also believed to be the cause of certain anomalous behaviors in the thermodynamic properties of glasses in the $10-30$ K range. Although the boson peak has been the subject of much work, its origin remains controversial. Theoretical investigations of the boson peak, which can be directly compared to the results presented here, include molecular-dynamics simulations of vitreous silica,[20,21] a soft-sphere glass,[22] and the unit density Lennard-Jones glass.[23] These studies tend to suggest that the vibrations responsible for the boson peak are (quasi)localized and anharmonic, although Mazzacurati *et al.* suggested that the low-frequency vibrations in a Lennard-Jones system were best described as a combination of uncorrelated random motion and well-defined sinusoidal waves.[23]

A number of simulations and experiments have suggested that the low-frequency modes in silica that contribute to the boson peak can be described as strongly anharmonic, localized relative rotation of coupled SiO_4 tetrahedra.[18,21,24–26] The boson peak is almost a universal characteristic of glasses, although its intensity tends to decrease with increasing fragility.[6] Das has recently suggested that this correlation is due to the speed at which defects relax: long-lived defects in strong glasses might give rise to extra intensity at an intermediate frequency following the quasielastic Raman peak.[27] He proposed that in fragile liquids the defects have a shorter lifetime, and so have less effect in the intermediate-frequency range.

Two-level systems have been suggested as the cause of the anomalous specific heat and thermal conductivity of glasses in the $0-10$ K region.[28–30] A two-level system is a pair of minima separated by a barrier that produces a splitting of around 1 K, after tunneling has been taken into account.[31] Angell has noted that anomalous behavior in the $0-10$ K and $10-30$ K regions tend to occur together if they are seen at all,[32–34] and inferred that the same low-frequency, anharmonic modes are associated with the boson peak and two-level systems. It is certainly conceivable that the potential will be very anharmonic at the bottom of a minimum that is connected to a low-lying transition state, as is the case in a two-level system. In the present work we have also investigated Angell's hypothesis by searching along the eigenvector corresponding to the softest eigenvalue to see if it leads to a low-lying transition state (Sec. IV D).

The inherent structure method developed by Stillinger and Weber has previously been used to analyze the behavior of glassy systems in the ''landscape dominated'' regime. The inherent structure of a configuration is the local minimum reached by following the steepest-descent path.[35] Monitoring the transitions between inherent structures in simulations confirmed the existence of slow barrier crossings and localized rearrangements at low temperatures, as described in the Goldstein picture.[36]

Following Jonsson and Anderson,[37] Sastry *et al.* inferred a variation in the barrier distributions for the binary Lennard-Jones glass from molecular-dynamics (MD) simulations.[38] Configurations were quenched to local minima—their inherent structures—during a series of cooling runs following equilibration. The system was found to explore lower-energy regions of the PES as the temperature decreased, and lower regions were accessed for slower cooling rates, as expected. Inherent structures obtained from the runs at different temperatures were raised to a series of excitation temperatures T_e. The variation in barrier height was inferred from the mean-square distance in configuration space through which the system moved in a given time. However, the mean-square distance moved cannot be a simple function of the barrier distribution alone; it is also determined by the connectivity. A key aspect of the present contribution is that this missing factor is properly accounted for: we calculate the barriers for elementary rearrangements involving a single transition state to high precision.

Barkema and Mousseau have used their activation-relaxation technique[39] (ART) to generate local minima and approximations to saddle points for amorphous silicon[40–42] (a-Si) and silica.[43,44] They obtained a barrier distribution for a-Si with a maximum at around 2.0 eV and an estimated

error of ± 0.5 eV.[40,41] Experimental results from conductivity measurements[45] and differential calorimetry[46] give activation energies for these transport processes of around 1–2 eV for *a*-Si.

Recently, some other groups have also addressed the relation between the PES and global dynamics in terms of periodic Lennard-Jones systems modeled by small supercells.[47–50] We have conducted brief surveys of these systems and have found many times more stationary points than were previously reported, giving us further confidence in the well-established methods used in the present work.[8] For comparison, transition states are located between two and three orders of magnitude faster for small systems than with another recently proposed recipe.[51]

II. POTENTIALS

Four systems are considered in the present work, as detailed below. In each case we adopt the natural reduced unit system, where energy is measured in ϵ and length in σ (ϵ_{AA} and σ_{AA} for binary Lennard-Jones). The corresponding reduced unit of time is $\sqrt{m\sigma^2/\epsilon}$, and unit masses were also employed throughout. In each case the energy unit corresponds to the pair well depth and $2^{1/6}\sigma$ corresponds to the pair equilibrium separation (for *A*-*A* interactions in the binary Lennard-Jones system). Reduced temperatures are defined by k_BT/ϵ and the unit of frequency is $\sqrt{\epsilon/m\sigma^2}$. Since supercells of different sizes are used for different systems the energies of local minima will be reported in ϵ per atom. However, barrier heights, which are not expected to be extensive quantities, will be reported in ϵ per supercell.

A. Binary, unit density, and relaxed Lennard-Jones solids

The Lennard-Jones (LJ) potential[52] for two atoms separated by a distance r is given by

$$V(r)=4\epsilon\left[\left(\frac{\sigma}{r}\right)^{12}-\left(\frac{\sigma}{r}\right)^{6}\right], \tag{2}$$

where ϵ is the depth of the potential energy well, and $2^{1/6}\sigma$ is the pair equilibrium separation.

Our unit density Lennard-Jones system (ULJ) contained 256 atoms and has hexagonal-and face-centered-cubic close-packed crystalline minima (hcp and fcc). The relaxed Lennard-Jones (RLJ) system has a box length optimized for the fcc solid with a number density of $0.93\,\sigma^{-3}$, indicating that the ULJ crystal corresponds to a large negative pressure. The cutoff employed for both these systems was 3.17σ.

The binary Lennard-Jones system (BLJ) is commonly used because it does not crystallize in simulations. It consists of 205 (80%) *A* atoms and 51 (20%) *B* atoms, with parameters $\sigma_{AA}=1.0$, $\sigma_{AB}=0.8$, $\sigma_{BB}=0.88$, $\epsilon_{AA}=1.00$, $\epsilon_{AB}=1.5$, and $\epsilon_{BB}=0.5$. The units of distance and energy were taken as σ_{AA} and ϵ_{AA}. The box length used for the periodic boundary conditions was set to give a number density of $1.2\,\sigma_{AA}^{-3}$, and a cutoff of $2.5\,\sigma_{\alpha\beta}$ was used, where α, β are *A* or *B*. All these parameters are the same as those employed by Sastry *et al.*,[38] and we employed the shifting and truncation scheme of Stoddard and Ford.[120] This system has been proposed as a model for the metallic glass $Ni_{0.8}P_{0.2}$, which has also been simulated[53] using a two-body term of the same form as that of the Stillinger-Weber silicon potential. Lennard-Jones models have been used extensively in the study of ageing phenomena[54,55] and mode-coupling theory.[56]

B. The Stillinger-Weber (SW) silicon potential

The Stillinger-Weber (SW) silicon potential[57] has two- and three-body contributions:

$$\nu_2(r_{ij})=\epsilon f_2\left(\frac{r_{ij}}{\sigma}\right), \quad \nu_3(\mathbf{r}_i,\mathbf{r}_j,\mathbf{r}_k)=\epsilon f_3(\mathbf{r}_i,\mathbf{r}_j,\mathbf{r}_k). \tag{3}$$

ϵ and σ are chosen so that the minimum value of f_2 is $f_2(2^{1/6})=-1$, and f_2 and f_3 are given by

$$f_2(r)=\begin{cases} A(Br^{-p}-r^{-q})\exp(r-a)^{-1}, & r<a, \\ 0, & r\geqslant a, \end{cases} \tag{4}$$

$$f_3(\mathbf{r}_i,\mathbf{r}_j,\mathbf{r}_k)=h(r_{ij},r_{jk},\theta_{jik})+h(r_{ji},r_{jk},\theta_{ijk}) +h(r_{ki},r_{kj},\theta_{ikj}), \tag{5}$$

$$h(r_{ij},r_{jk},\theta_{jik})=\lambda\,\exp[\gamma(r_{ij}-a)^{-1}+\gamma(r_{ik}-a)^{-1}] \times\left(\cos\theta_{ijk}+\frac{1}{3}\right)^2. \tag{6}$$

Stillinger and Weber used best-fit parameters of $A=7.050$, $B=0.6022$, $p=4$, $a=1.80$, $\lambda=21.0$, $\gamma=1.20$, $\sigma=2.0951$ Å, and $\epsilon=2.1682$ eV. The box length for the 216-atom supercell used here is $7.776\,643\,\sigma$, the optimum value for the crystal at zero pressure, and the potential has a built-in cutoff at $a=1.80\,\sigma$.

It has been suggested that the three-body term ν_3 should be increased by 50%.[39,40] This modification is believed to give a more appropriate structure for *a*-Si and amorphous germanium.[58] One of our databases, denoted SW1.5, was obtained using this modification, as described in Sec. III.

III. CHARACTERIZATION OF POTENTIAL ENERGY SURFACES

Previously, for small clusters, it has been possible to perform an exhaustive search of the PES for stationary points.[8] Empirically, the number of minima of a system of N atoms increases roughly as $2N!\exp(\alpha N)$,[35,59–61] making an exhaustive search of the PES for large systems impossible. We must therefore consider incomplete databases of minima and transition states. Such incomplete databases should be representative of the region of the PES that is explored by the system under experimental conditions.

The methods employed in the present work are broken down into three subsections below. The geometry optimization and pathway characterization techniques have been described before, and a brief summary is presented in Sec. III A. For each system we generated one or more databases of connected minima, transition states, and rearrangement pathways. Each such database requires an initial minimum, and these choices are described in Sec. III C and Appendix

B. Given a starting point, the databases were constructed using algorithms similar to those we have employed before in studies of finite systems, as summarized in Sec. III B and Appendix A.

A. Stationary point searches

Stationary points on a PES are points where the gradient vector vanishes. A minimum is a stationary point with no negative Hessian eigenvalues (no imaginary normal-mode frequencies). In the present work we follow Murrell and Laidler and define a true transition state as a stationary point with precisely one negative Hessian eigenvalue (one imaginary normal-mode frequency). For each transition state two barrier heights are then determined by the energy differences between the transition state and the two minima that are connected to it by steepest-descent paths. As usual, we will refer to the larger barrier for a given transition state as the uphill barrier, because it must be overcome to move from the lower- to the higher-energy minimum. Similarly, the smaller barrier is referred to as the downhill barrier.

The systems studied here are large enough to make eigenvector-following[62–65] transition state searching techniques rather expensive.[66–68] Newly developed hybrid eigenvector-following algorithms were therefore used to find the transition states.[68] These techniques avoid diagonalizing the Hessian matrix at every step, which is the computational bottleneck for the present potentials in systems of this size. The most efficient method derives from the eigenvector-following conjugate-gradient (EF/CG) approach described elsewhere,[67] where the Hessian is calculated analytically and the eigenvector corresponding to the lowest nonzero eigenvalue is obtained by shifting and iteration. Uphill steps are taken in this eigendirection using the implementation of eigenvector following described elsewhere.[65,66,69,70] Minimization is performed in the tangent space between eigenvector-following steps, and a significant speed-up was obtained using Nocedal's limited memory BFGS routine[71] instead of conjugate-gradient minimization.[72] We therefore refer to this technique as EF/BFGS. The present calculations allowed up to 100 iterations in the calculation of the smallest Hessian eigenvalue, up to 100 iterations in the calculation of the largest eigenvalue, and 10 BFGS steps in the subspace minimization before the smallest eigenvalue had converged and 100 thereafter. The smallest eigenvalue was deemed to have converged when it changed by less than 0.01% between successive steps. Initial diagonal elements of the inverse Hessian were set to $0.1\,\sigma^2\epsilon^{-1}$.

In order to find more than one transition state connected to a given minimum we have previously employed search directions along Hessian eigenvectors corresponding to increasing Hessian eigenvalues.[8] However, this procedure results in frequent duplication, and Malek and Mousseau found it more efficient to use random search directions.[73] We initially employed the simple expedient of randomly perturbing the initial minimum before searching uphill along the eigenvector corresponding to the smallest nonzero Hessian eigenvalue. However, a more efficient method was subsequently developed, which is described in Appendix A. All the results presented below employed the new approach.

For each transition state the corresponding pathway was calculated using Nocedal's BFGS scheme[71] following suitable small displacements of order 0.01 parallel and antiparallel to the reaction vector. The resulting pathways should be a good enough approximation to the true steepest-descent paths for the present purposes.

A small number of full eigenvector-following steps (between one and three) were used to converge all the stationary points to a root-mean-square (RMS) force of less than 10^{-6} reduced units. This precaution, which involves full diagonalization of the analytic Hessian matrix, also assures us that the stationary points in question have the correct number of negative Hessian eigenvalues, namely, zero for a minimum and one for a true transition state. For an RMS force less than 10^{-6} units the energies per supercell are converged to better than ten significant figures for all the stationary points.

B. Sampling schemes

Various approaches have been described for systematically exploring a PES by moving between local minima.[8,39,74–76] Starting from a known minimum we conducted transition state searches using hybrid eigenvector-following and the scheme described in Appendix A. For each new transition state the corresponding pathway was calculated. If neither of the connected minima corresponded to the minimum from which the transition state was found, the path was discarded. New connected minima were added to the database and were subsequently used as starting points for transition state searches in the same way, in order of increasing energy. For each database searching was terminated when 10 000 connected transition states had been found. The minima in each set are therefore also connected, i.e., any pair can be interconverted via a series of transition states from the same database. This condition is important for future dynamical studies and for the construction of disconnectivity graphs.[8]

In the present work we constructed some databases using a maximum of eight transition state searches from each minimum, moving to a new connected minimum if it had lower energy than the one from which the transition state was found. Other databases were generated using 400 transition state searches from each minimum, starting from a new minimum only after all 400 searches were complete. Comparing data sets generated with these alternative parameters should tell us whether the barrier distributions obtained are sensitive to the sampling technique. The first sampling scheme (SS1) provides an overview of a wide range of configuration space, while the second (SS2) probes a smaller region more thoroughly. A third sampling scheme, SS3, was used to generate intermediate databases (see Appendix B) and to create the largely crystalline Stillinger-Weber and ULJ databases SW(x) and ULJ(x). In SS3 we employed up to 40 transition state searches per minimum, accepting downhill moves to new connected minima as for SS1. SW(x) and ULJ(x) were created to calculate vibrational densities of states (VDOS) for comparison with the disordered VDOS (Sec. IV D). SS3 was chosen as a compromise between SS1 and SS2. Attempts to generate databases using SS1 and SS3

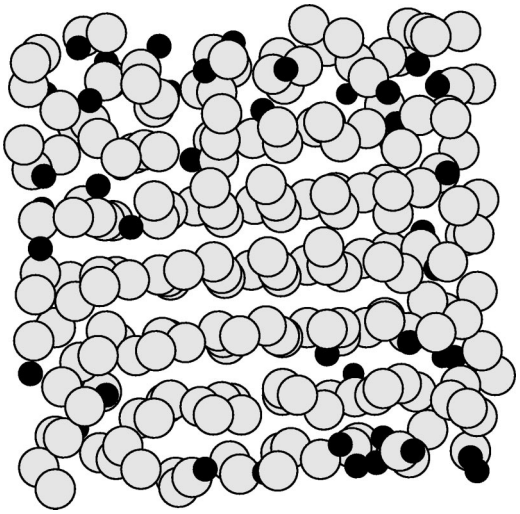

FIG. 1. Lowest-energy minimum found for the binary Lennard-Jones (BLJ) system, showing significant ordering of the larger *A* atoms and some degree of phase separation.

from starting minima with residual regions of crystalline structure inevitably led to the crystal being located within the first few hundred minima. This is the expected behavior for homogeneous Lennard-Jones systems,[77] and the disconnectivity graphs illustrated in Sec. III D show that the crystal is readily located once a critical nucleus is present.

C. Selection of starting configurations for database generation

Our most extensive results are for the BLJ system, which has recently been the subject of several other studies.[38,78–86] We also chose this system to test the dependence of the final databases of stationary points on the starting minimum and on the two sampling schemes SS1 and SS2, described in Sec. III B above. Since the lowest minimum is not known for BLJ we first decided to run a ''basin-hopping'' global optimization search.[87] In this procedure the energy at a point in configuration space becomes the energy of the ''nearest'' minimum, transforming the PES into a collection of plateaus or basins of attraction.[88] The transformed landscape was explored starting from phase-separated atoms on fcc lattice sites using Monte Carlo sampling of the transformed landscape at a temperature of $0.8\,\epsilon_{AA}$. The random displacement of atomic coordinates for proposed steps was adjusted to give an acceptance ratio of about 0.5. Figure 1 shows the lowest minimum located in a run of 20 000 basin-hopping steps. Another global optimization run of the same length was performed, this time starting from the lowest-energy minimum obtained by systematic quenching from a molecular-dynamics (MD) trajectory at an energy of $-5.8594\,\epsilon_{AA}$ per atom, but it did not produce a lower minimum. For a system of this complexity locating the global minimum reliably would require much longer basin-hopping runs than we have used here—we can only be confident that relatively low-energy minima have been found. It is therefore not surprising that the two global optimization runs did not converge to the same structure. Rather, this result suggests that the very lowest minima will probably exhibit some phase separation and will be rarely sampled in an MD simulation of the liquid.

Our results may be compared with the energy obtained by Angell *et al.*'s extrapolation[78] of Sastry and coworkers' excitation profile.[38] Using the assumption that the critical temperature of mode-coupling theory T_c and the Kauzmann temperature T_K are related by $T_c/T_K \sim 1.6$, Angell *et al.* obtained an energy of about $-7.08\,\epsilon_{AA}$ per atom, that agrees reasonably well with the value of $-7.0541\,\epsilon_{AA}$ per atom for our lowest-energy minimum. The latter structure (Fig. 1) appears to be a close-packed arrangement of *A* atoms, with *B* atoms arranged interstitially and substitutionally. There is a degree of phase separation, with the *B* atoms more concentrated near the top and bottom of the supercell. Hence the most stable structure for this system seems to be lamellar, although obviously the thickness of the lamellae will be strongly affected by the size of the supercell and the number density of atoms.

Database BLJ1 was obtained using SS1 (up to eight searches per minimum) by starting from the lowest-energy BLJ minimum described above. Databases BLJ2 and BLJ3 were generated using SS1 starting from two of the minima obtained by quenching at regular time intervals of $\sqrt{m\sigma_{AA}^2/\epsilon_{AA}}$ from an MD trajectory of length $1000\sqrt{m\sigma_{AA}^2/\epsilon_{AA}}$ run at a total energy of $-3.906\,\epsilon_{AA}$ per atom. The energies of the starting minima for the two samples were selected to produce databases of minima that fully span the range of inherent structure energies studied by Sastry *et al.*[38] Apart from this consideration, the selection of these two starting minima was random.

To check the dependence of the databases upon the sampling scheme and the starting minimum we generated databases BLJ4–10 using SS2 (400 searches per minimum). The starting minima were selected randomly from databases BLJ1-3, except that their energies were chosen to span the full range of the latter databases, and the BLJ4 starting configuration was the low-energy minimum used as the starting point for BLJ1.

As one final check of the statistics we generated databases BLJ11–14 using SS2 and starting minima obtained from a further set of short MD trajectories suggested by the cooling schedules of Sastry *et al.*[38] The system was initially equilibrated for 5000 steps at a total energy of $-1.875\,\epsilon_{AA}$ per atom, with a time step of $0.003\sqrt{m\sigma_{AA}^2/\epsilon_{AA}}$. It was then cooled by successive runs of 100 steps at progressively lower total energies. The energy was reduced each time by $0.071\,88\,\epsilon_{AA}$ per atom by rescaling the velocities, corresponding to a cooling rate of $4.219\times10^{-3}\sqrt{\epsilon_{AA}/m\sigma_{AA}^2}$ per atom. This schedule corresponds to the fastest rate used by Sastry *et al.* Cooling was continued until the total energy was essentially equal to the potential energy of the (unquenched) configuration. Databases BLJ11–14 correspond to configurations obtained from MD trajectories at total energies of $-6.8344\,\epsilon_{AA}$, $-5.3969\,\epsilon_{AA}$, $-4.6781\,\epsilon_{AA}$, and $-2.1625\,\epsilon_{AA}$ per atom, respectively, which correspond to steps in the above cooling schedule.

TABLE I. Details of the databases studied. E_1 is the energy of the initial minimum, E_{low} and E_{high} are the energies of the lowest- and highest-lying minima, and N_{min} is the number of minima in the database. Each sample contains 10 000 transition states. All the energies are in ϵ per atom (Sec. II). $\langle E_{\mathrm{min}} \rangle$ and $\langle E_{\mathrm{ts}} \rangle$ are the mean energies of the minima and transition states, respectively.

Database	E_1	E_{low}	E_{high}	N_{min}	$\langle E_{\mathrm{min}} \rangle$	$\langle E_{\mathrm{ts}} \rangle$
Binary Lennard-Jones, sampling scheme SS1						
BLJ1	−7.0541	−7.0541	−6.8546	9275	−6.9784	−6.9695
BLJ2	−6.9377	−6.9811	−6.8280	9485	−6.9197	−6.9115
BLJ3	−6.8560	−6.9846	−6.8185	9571	−6.9176	−6.9097
Binary Lennard-Jones, sampling scheme SS2, starting minima from BLJ1–3						
BLJ4	−7.0541	−7.0541	−6.9285	7867	−7.0070	−6.9930
BLJ5	−7.0336	−7.0444	−6.9206	8126	−6.9949	−6.9802
BLJ6	−7.0137	−7.0514	−6.8958	8161	−6.9889	−6.9766
BLJ7	−6.9948	−7.0242	−6.8906	8455	−6.9737	−6.9605
BLJ8	−7.0016	−7.0220	−6.8916	8434	−6.9694	−6.9564
BLJ9	−6.9531	−6.9716	−6.8519	8435	−6.9277	−6.9155
BLJ10	−6.9350	−6.9585	−6.8218	8810	−6.9131	−6.9013
Binary Lennard-Jones, sampling scheme SS2, starting minima from MD cooling runs						
BLJ11	−6.9723	−6.9846	−6.8699	8419	−6.9356	−6.9235
BLJ12	−6.9439	−6.9734	−6.8434	8708	−6.9245	−6.9124
BLJ13	−6.9218	−6.9598	−6.8252	8674	−6.9029	−6.8900
BLJ14	−6.8936	−6.9427	−6.8177	9109	−6.8866	−6.8745
Unit density Lennard-Jones, sampling scheme SS2						
ULJ1	−7.3444	−7.3456	−7.2186	4460	−7.3141	−7.3038
ULJ2	−7.2513	−7.3456	−7.1579	7541	−7.2595	−7.2349
ULJ3	−7.0147	−7.3957	−6.9774	9212	−7.0580	−7.0319
Relaxed Lennard-Jones, sampling scheme SS2						
RLJ1	−6.9711	−7.4908	−6.8775	8355	−7.0614	−7.0005
RLJ2	−6.9072	−7.7067	−6.8751	8249	−7.0512	−7.0392
Stillinger-Weber Si, sampling scheme SS2						
SW1	−1.8949	−1.8966	−1.8838	6939	−1.8921	−1.8920
SW2	−1.8796	−1.8857	−1.8779	5834	−1.8807	−1.8803
SW3	−1.8631	−1.8750	−1.8623	5883	−1.8660	−1.8654
Adjusted Stillinger-Weber Si potential, sampling scheme SS2						
SW1.5	−1.8496	−1.8892	−1.8251	8716	−1.8485	−1.8452
Largely crystalline ULJ and SW samples, sampling scheme SS3						
SW(x)	−1.9937	−2.0000	−1.9601	7664	−1.9784	−1.9777
ULJ(x)	−7.5392	−7.5392	−7.2473	3367	−7.3641	−7.3619

Having determined that the properties of each database are relatively insensitive to the sampling scheme for the BLJ system (Sec. IV A) we generated databases for the other three model glasses more selectively, as described in Appendix B. Table I contains some statistics for each of the databases.

D. Crystallinity

The Stillinger-Weber and homogeneous Lennard-Jones systems have crystalline global minima, diamond and hcp, respectively, for zero external pressure. We have used an order parameter introduced by Steinhardt *et al.* to measure the degree of crystallinity in our samples.[89] These order parameters are based on the square of the sums of spherical harmonics for all N_b bonds in the supercell, using the minimum image convention. The value of the order parameter is slightly sensitive to the choice of the cutoff that determines which atoms are bonded: the value we used was 1.24 times the nearest-neighbor distance for the fcc structure, as in previous work.[90]

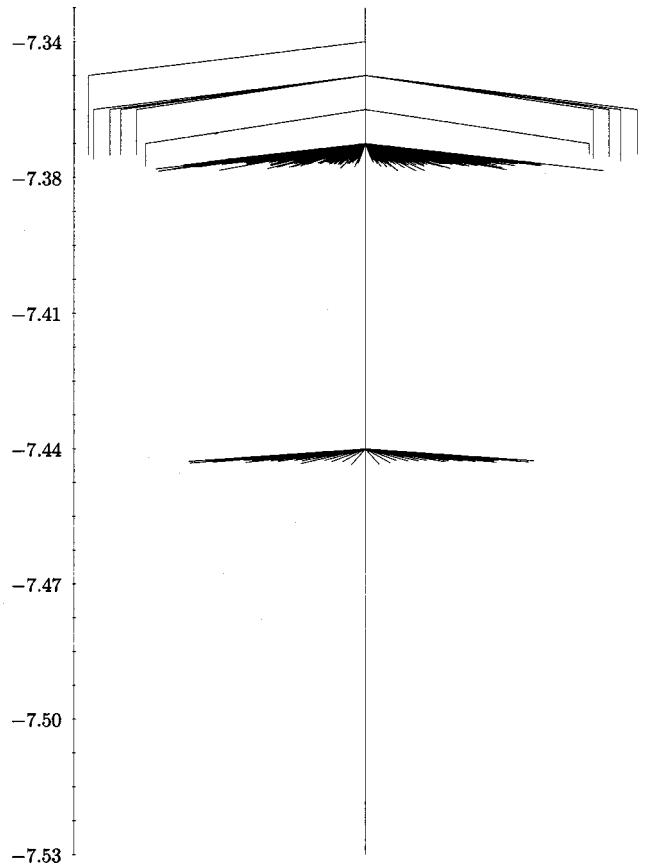

FIG. 2. Disconnectivity graph containing the lowest 500 minima for the unit density Lennard-Jones system ULJ(x). Energies are in ϵ per atom.

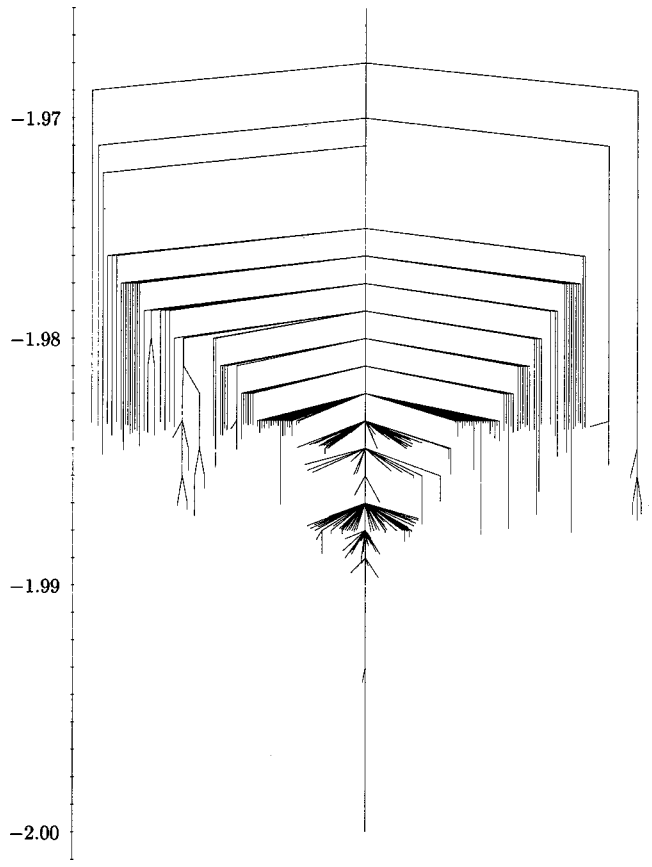

FIG. 3. Disconnectivity graph containing the lowest 850 minima for the Stillinger-weber silicon system SW(x). Energies are in ϵ per atom.

The most appropriate order parameter for our purposes is based on sixth-order spherical harmonics, and is denoted Q_6. It is particularly useful, as it vanishes for the liquid and has a similar value for all common crystalline structures, namely, 0.574 52 for fcc, 0.484 76 for hcp, and 0.510 69 for body-centered cubic. Thus, values close to zero represent a disordered structure, while values of order $0.4-0.5$ are indicative of crystalline order.

The average values of Q_6 for our ULJ samples are 0.45 for ULJ1, 0.46 for ULJ2, and 0.17 for ULJ3. All the values for the BLJ samples are less than 0.1, and those for RLJ1 and RLJ2 are 0.24 and 0.21, respectively. Q_6 is not applicable as a measure of crystallinity for tetrahedral coordination, so we did not use it for the SW system.

Disconnectivity graphs[91] for the low-energy regions of samples ULJ(x) and SW(x) are shown in Figs. 2 and 3, respectively. Such graphs have recently been employed to visualize the many-dimensional PES in a variety of systems.[8,91–94] At a series of discrete energies the minima are grouped into disjoint sets, whose members are mutually accessible at that energy via known transition states. Each set is represented by a node, and lines are drawn between the nodes to indicate how the sets split as the energy is decreased. All these lines ultimately terminate at local minima, whose positions are determined by their energy on the vertical scale. The horizontal position of the nodes is arbitrary and can be chosen for clarity. Further details and examples may be found elsewhere.[8,91] Figures 2 and 3 reveal a ''palm-tree''-type structure for these low-energy regions of the two surfaces,[8,92] where minima are disconnected gradually as the total energy decreases. Relaxation to the crystal will clearly proceed rapidly from any of the minima included in these trees.

IV. PROPERTIES OF THE POTENTIAL ENERGY SURFACES

A. Barrier distributions

Every transition state is associated with an uphill (larger) and a downhill (smaller) barrier (Sec. III A), except for degenerate rearrangements[95] where the two are the same. We present the barrier height distributions using a Gaussian for each data point:

$$f(b)=\frac{1}{n}\sum_{i=1}^{n}\frac{e^{-(b-b_i)^2/2s^2}}{\sqrt{2\pi s^2}}.$$

This convolution produces a smooth function when the Gaussian width s is chosen appropriately. An approximate representation of the probability distribution $f(b)$ for the barrier height b is thereby obtained from the n observed barrier heights b_i in the database.

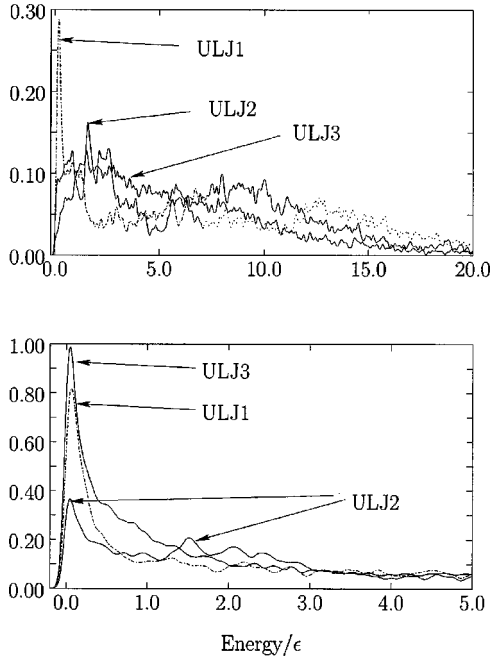

FIG. 4. Uphill (top panel) and downhill (bottom panel) barrier distributions for the unit density Lennard-Jones (ULJ) databases. The Gaussian width used to construct the distribution was $s = 0.05\,\epsilon$ and the barriers are in ϵ per supercell. The negative-energy tail is caused by the Gaussian smoothing procedure used to construct the distribution function.

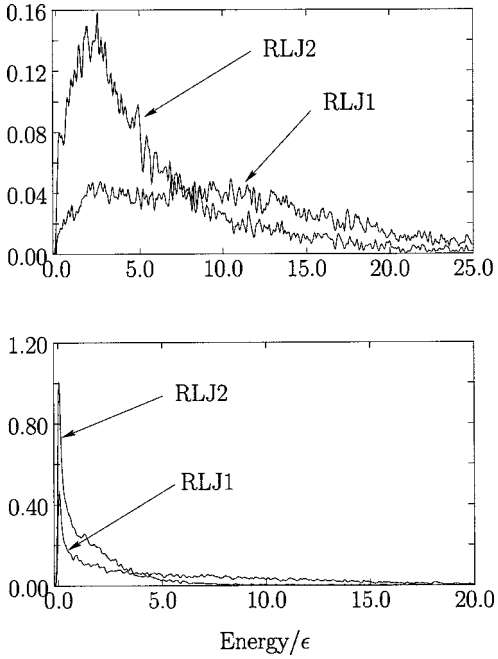

FIG. 5. Uphill (top panel) and downhill (bottom panel) barrier distributions for the relaxed Lennard-Jones (RLJ) databases. The Gaussian width used to construct the distribution was $s = 0.05\,\epsilon$ and the barriers are in ϵ per supercell.

We will focus on the downhill (Sec. III A) barrier distributions for brevity. For any pathway the uphill barrier is equal to the downhill barrier plus the energy difference between the higher- and the lower-lying minima. The uphill barrier distribution is therefore largely determined by the distribution of energy differences between minima. We also expect relaxation towards equilibrium to be more dependent upon the downhill barrier distribution.

Uphill and downhill barrier distributions for the different databases are illustrated in Figs. 4–9. Table II summarizes the maxima in the uphill and downhill barrier distributions. For the most extensively investigated binary Lennard-Jones (BLJ) system it is apparent from Figs. 6–8 that there is no dramatic variation in the downhill barrier distributions we have obtained for different searching methods or choices of starting configuration.

Figure 7 shows that a smaller number of searches from each minimum tends to bias the distribution towards lower barriers. Databases BLJ1–3 were generated using SS1 with eight searches from each minimum; databases BLJ4–10 span the same energy range. The maxima in the downhill barrier distributions in Table II are similar for all the data sets, varying between about $0.03-0.05\,\epsilon_{AA}$ per supercell. The uphill barrier distributions of samples BLJ1–10 are all quite similar and cover the range $0-20\,\epsilon$ per supercell. Note that we report barrier heights as energy differences per supercell, since the relevant barriers should not scale extensively with system size. The estimated barrier of $5\,\epsilon_{AA}$ obtained in another recent study[86] is consistent with our results. The low barrier processes that dominate our downhill barrier distributions do not seem to have been noticed before, however.[85,86]

It may seem surprising that the barrier distributions are quite similar for all the BLJ samples (except BLJ1), since

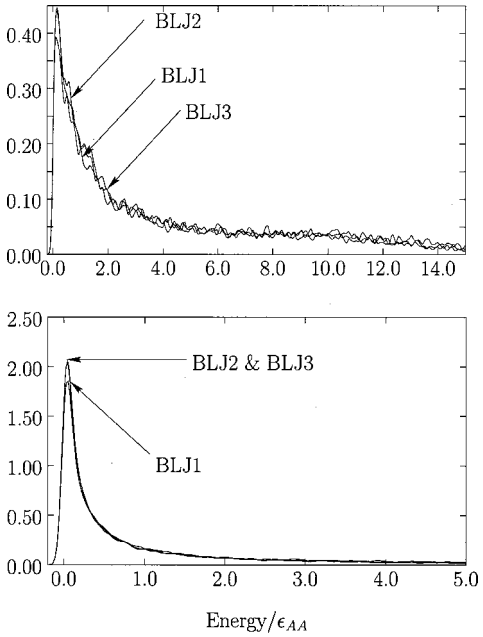

FIG. 6. Uphill (top panel) and downhill (bottom panel) barrier distributions for binary Lennard-Jones (BLJ) databases BLJ1–3 generated using the first sampling scheme SS1 described in Sec. III B (maximum of eight transition state searches per minimum). The Gaussian width $s = 0.05\,\epsilon_{AA}$ and the barriers are in ϵ_{AA} per supercell.

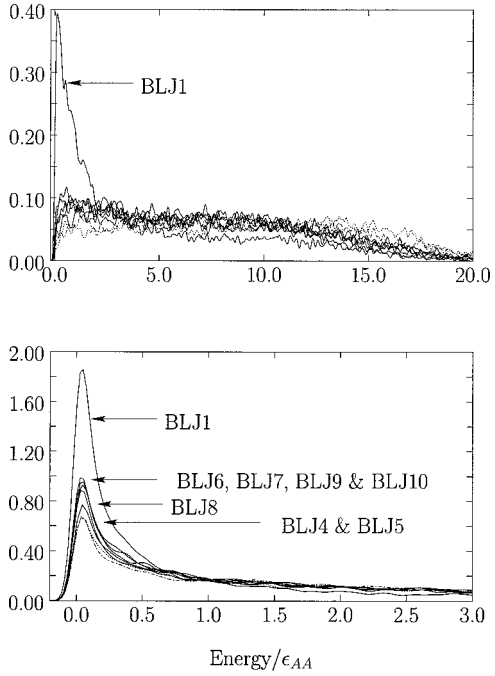

FIG. 7. Uphill (top panel) and downhill (bottom panel) barrier distributions for binary Lennard-Jones (BLJ) databases BLJ5–10 generated using the second sampling scheme SS2 described in Sec. III B (400 transition state searches per minimum). Database BLJ1 is included for comparison. The Gaussian width $s=0.05\,\epsilon_{AA}$ and the barriers are in ϵ_{AA} per supercell.

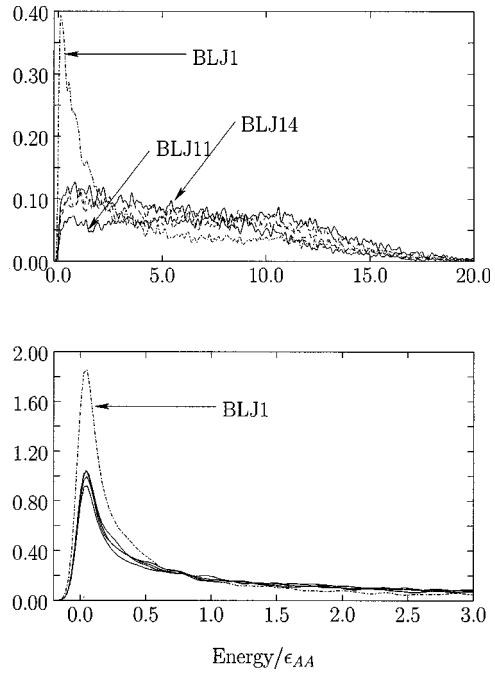

FIG. 8. Uphill (top panel) and downhill (bottom panel) barrier distributions for the binary Lennard-Jones (BLJ) databases BLJ11–14 generated using sampling scheme SS2 (Sec. III B) (400 transition state searches per minimum) and starting minima derived from an MD cooling run. The Gaussian width $s=0.05\,\epsilon_{AA}$ and the barriers are in ϵ_{AA} per supercell.

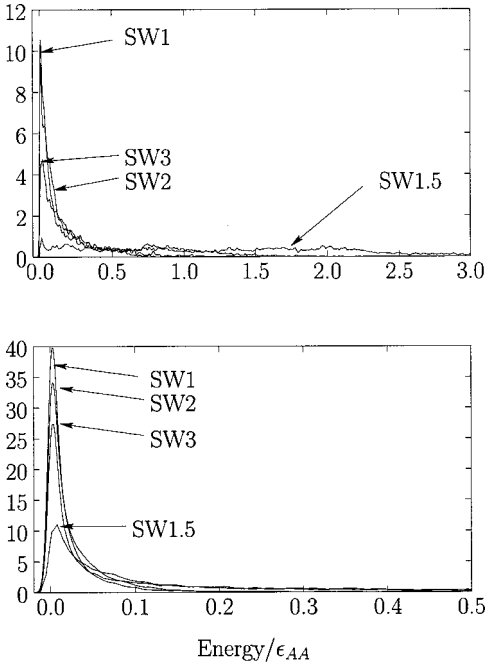

FIG. 9. Uphill (top panel) and downhill (bottom panel) barrier distributions for the Stillinger-Weber databases SW1–3 and for the modified Stillinger-Weber potential SW1.5 (Sec. II B). The Gaussian width $s=0.005\,\epsilon$ and the barriers are in ϵ per supercell.

Sastry *et al.*[38] inferred that the barriers increase in magnitude as the system explores lower energy regions of the PES for this system. However, it is probably the case that the ''barriers'' observed by Sastry *et al.* correspond to the total activation energy for multistep processes rather than to single rearrangements. Our results are supported by the work of Kopsias and Theodorou, who found that the free energy barrier heights for a 198-atom homogeneous Lennard-Jones system[96] were independent of the free energies of the minima involved.

Both Fig. 9 and Table II show that all the uphill and downhill barrier distributions for Stillinger-Weber (SW) silicon exhibit pronounced maxima at rather low energies of $0.002-0.02\,\epsilon$ per supercell or $0.004-0.04$ eV. This result contrasts with the peak at around 2 eV found by Barkema and Mousseau,[40,42] although their distributions also have significant amplitude at low energy. They ascribed the low barriers to the presence of ''unstable'' minima in their sample, although our results suggest that these low barriers are rather ubiquitous, at least under constant volume conditions. It is possible that the approximations involved in finding transition states by the original activation-relaxation technique (ART) produce a bias towards high-energy barriers. The present results are converged to much higher precision, albeit for smaller supercells, and may lead to a bias towards rearrangements with low-energy barriers. Malek and Mousseau[73] have subsequently employed a hybrid eigenvector-following technique that we would expect to produce essentially equivalent results to ours if the PES is sampled in the same way.

The low-energy peaks that we have found in the barrier distributions for the SW silicon potentials do not appear to

TABLE II. Mean values of the integrated path lengths $\langle S \rangle$ in σ (Sec. II), separations of connected minima $\langle D \rangle$ in σ, and cooperativity indices $\langle \tilde{N} \rangle$ for all the databases studied. These quantities are defined in Sec. IV C. $E_{\max}$(up) and $E_{\max}$(down) are the energies of the largest maxima in the distributions of uphill and downhill barriers, respectively, in ϵ per supercell.

Database	$\langle S \rangle$	$\langle D \rangle$	$\langle \tilde{N} \rangle$	$E_{\max}$(up)	$E_{\max}$(down)
Binary Lennard-Jones, sampling scheme SS1					
BLJ1	4.13	1.47	5.58	0.0992	0.0508
BLJ2	4.48	1.59	8.18	0.1463	0.0508
BLJ3	4.46	1.60	8.40	0.1466	0.0456
Binary Lennard-Jones, sampling scheme SS2, starting minima from BLJ1–3					
BLJ4	5.99	1.88	4.71	5.3148	0.0340
BLJ5	5.79	1.84	4.51	5.1701	0.0388
BLJ6	6.14	1.91	6.68	0.5588	0.0548
BLJ7	6.50	1.96	6.80	0.6800	0.0328
BLJ8	5.77	1.82	5.17	4.6648	0.0450
BLJ9	6.72	2.01	7.86	0.2883	0.0302
BLJ10	6.96	2.13	9.88	0.7376	0.0499
Binary Lennard-Jones, sampling scheme SS2, starting minima from MD cooling runs					
BLJ11	7.11	2.12	8.06	10.6110	0.0545
BLJ12	7.08	2.11	10.09	0.9995	0.0504
BLJ13	7.24	2.18	10.84	1.0845	0.0490
BLJ14	6.80	2.14	11.19	0.7874	0.0449
Unit density Lennard-Jones, sampling scheme SS2					
ULJ1	3.91	1.57	2.74	0.1709	0.0614
ULJ2	5.92	2.02	3.50	1.5680	0.0480
ULJ3	12.30	3.54	36.53	1.5038	0.0521
Relaxed Lennard-Jones, sampling scheme SS2					
RLJ1	13.25	3.57	22.96	6.9479	0.0490
RLJ2	9.11	3.05	45.85	2.5032	0.0440
Stillinger-Weber Si, sampling scheme SS2					
SW1	2.43	0.95	8.18	0.0201	0.0041
SW2	2.26	0.90	16.68	0.0064	0.0032
SW3	2.54	0.94	17.25	0.0063	0.0024
Adjusted Stillinger-Weber Si potential, sampling scheme SS2					
SW1.5	3.74	1.35	5.17	0.0137	0.0080

manifest themselves in previous experimental and theoretical studies,[40,41,45,46] and we will comment further on this observation in Sec. IV B. When the three-body term is increased by 50% in sample SW1.5, the downhill barrier distribution retains the same form, although the principal peak is broadened and the maximum is shifted to higher energy. The uphill barrier distribution is significantly affected, with the amplitude decaying steadily up to an energy of about $2.5\,\epsilon$ (5 eV).

Table II shows that databases SW1 and BLJ11 have anomalously high peaks in their uphill barrier distributions; the relatively flat distribution for BLJ11 accentuates this effect. The lowest minimum in sample SW1 lies only $0.0017\,\epsilon$ lower than the starting minimum, while for BLJ11 the difference is only $0.012\,\epsilon_{AA}$ (Table I), suggesting that these minima may lie in regions where there are few pathways with low-energy barriers that allow relaxation to minima of lower energy. This situation would arise if the minima are at the bottom of deep funnels[8] or the ''megabasins'' proposed by Stillinger.[15] In Stillinger's picture such features are expected to exist for the binary Lennard-Jones system, which is reasonably ''fragile,'' but not for silicon, which is ''strong.'' The maxima in the uphill barrier distributions at anomalously high energies suggest that the regions of configuration space in question are effective kinetic traps.

In fact, the way that databases BLJ11 and SW1 were gen-

erated probably explains the above observations. Database BLJ11 was started from the final configuration generated by an MD cooling run, as the temperature of the system approached zero. The starting configuration for SW1 is the lowest in energy from the intermediate SS3 database (see Appendix B), but has no atoms in a crystalline environment. Hence it would not be surprising if both starting configurations lie at the bottom of a funnel or a monotonic sequence basin.[8,97,98]

It is also noteworthy that database RLJ2 (for relaxed Lennard-Jones) contains a minimum of lower energy than any in RLJ1, despite being started at higher energy. Closer examination of the rearrangements in database RLJ2 revealed several highly asymmetric processes, with uphill barriers of order $100\,\epsilon$ and downhill barriers of order $1\,\epsilon$. The downhill processes lead to a large increase in the crystallinity order parameter Q_6 from around 0.1 to 0.4. This result reveals the presence of rapid crystallization from some regions of the PES, as seen in the disconnectivity graphs shown in Sec. III D.

The general trend of all the uphill barrier distributions, especially for RLJ1 and RLJ2, is that the barrier distributions corresponding to stationary points higher up the PES tend to be peaked at lower energy. This result, combined with the similar downhill barrier distributions, suggests that all of these glass formers have regions of their PES that act as effective kinetic traps, as expected.

Two previous studies[80,99] have reported correlated motion of atoms in successive rearrangements for BLJ systems, but we have not investigated this phenomenon in the present work. The results for ULJ are discussed in the following section.

B. Nondiffusive and diffusive rearrangements

The largest peaks in the overall barrier distributions that we have obtained are all at rather low energy. In particular, the results for Stillinger-Weber silicon contrast with Barkema and Mousseau's distributions for *a*-Si,[40,42,44] which tend to peak at around 2 eV. Experimental evidence suggests that there is a lower bound for the barrier to relaxation in *a*-Si of 0.23 eV.[45] In fact, all our samples include many rearrangements with much larger barriers than the peak in the distribution, and we now analyze these results in more detail.

There is a slight ''double-hump'' form to the barrier distributions for the unit and relaxed homogeneous Lennard-Jones systems (ULJ and RLJ, Figs. 4 and 5), with a principal maximum at an energy of about $0.1\,\epsilon$ per supercell and a subsidiary maximum or shoulder around an energy of $1.4\,\epsilon$ per supercell. The latter feature is particularly pronounced for the ULJ2 database. Although these features are not obvious, they prompted us to investigate the nature of the rearrangements contributing to different parts of the distributions in more detail. Examining animations of the rearrangement pathways revealed that the two maxima correspond to different processes. We describe the mechanisms corresponding to the principal maximum as ''nondiffusive:'' although atoms move, there is essentially no change in the nearest-neighbor coordination. These mechanisms are similar to the ''cage-rattling'' processes observed in a system of hard spheres by Doliwa and Heuer,[100] who suggested that they correspond to the ''fast'' β process observed in the region of T_c, the critical temperature of mode-coupling theory. These authors suggested that α processes correspond to mechanisms in which particles leave their cages. The rearrangements that we classify as nondiffusive are not strictly the same as cage rattling, because they do not correspond to vibration about a single potential minimum; instead they result from distinct minima separated by small barriers. Mechanisms corresponding to readjustments of ''tight'' cages—with radii similar to the mean nearest-neighbor distance—are unlikely to contribute significantly to diffusion or other transport processes, as there is no real change in the coordination of the atoms. This is why we refer to them as ''nondiffusive.''

All the rearrangements we have visualized indicate that mechanisms with barriers in the region of the second maximum or shoulder for RLJ and ULJ correspond to the movement of atoms between adjacent coordination shells, and these mechanisms are clearly ''diffusive.'' Intuitively this result makes sense, as the activation energy is of the order of ϵ per supercell, the pair well depth of the Lennard-Jones model. An example of a rearrangement similar to vacancy creation in crystalline solids[101,102] is illustrated in Fig. 10. Free volume in minimum 1 is changed into a vacancy in minimum 2. These rearrangements will contribute to diffusion much more than the nondiffusive processes, as the nearest-neighbor contacts change, although they entail higher activation energies.

The tails of the barrier distributions of the homogeneous Lennard-Jones systems ULJ and RLJ contain more exotic rearrangements, such as the one illustrated in Fig. 11, in which a pair of atoms exchange positions in a reasonably crystalline local environment. This degenerate rearrangement[95] (between permutational isomers) has a barrier of $18.7\,\epsilon$ (per supercell). A significant degree of bond stretching in the transition state is visible, while in other parts of the supercell, not shown in this figure, there must exist a corresponding degree of compression, resulting in a high barrier.

Nondiffusive rearrangements can be quite successfully separated from diffusive processes by counting the number of atoms whose positions at the end points of the rearrangement differ by a threshold value. The separation works for each mechanism that we have visualized, and the two distributions are also separated in terms of energy, as we would expect. This observation is true even for the BLJ and SW samples where there is no clear subsidiary feature in the barrier distribution. We classify nondiffusive rearrangements as those in which no atoms move by more than the threshold distance, and all other rearrangements are then assumed to be diffusive. A suitable threshold distance corresponds to about half the equilibrium pair separation, depending on the potential. Obviously, there are many rearrangements whose classification is sensitive to the precise value of the threshold distance, and in reality there exists a continuum between the ''diffusive'' and ''nondiffusive'' limits.

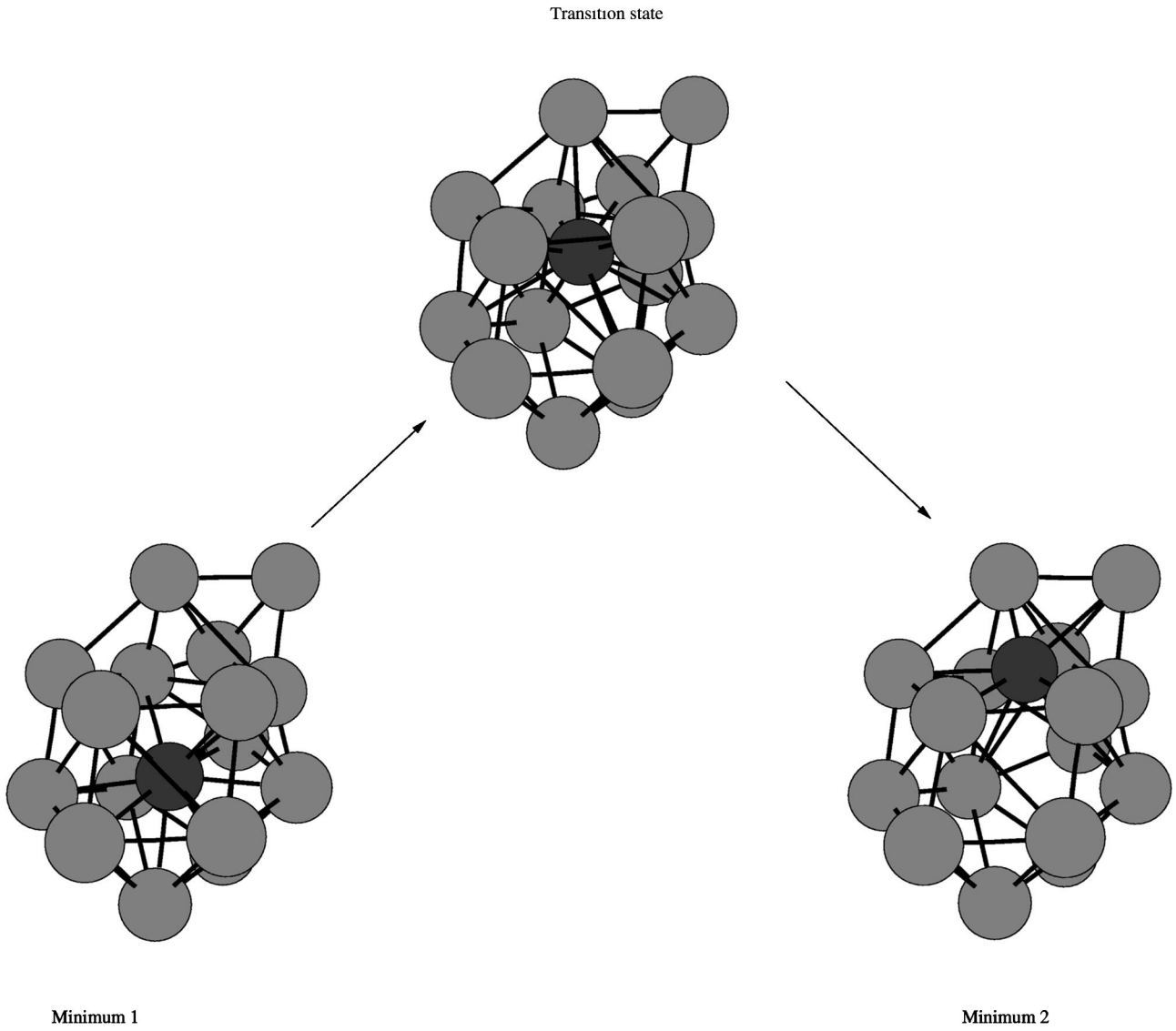

FIG. 10. Rearrangement illustrating a change in coordination of the highlighted atom and vacancy creation in unit density Lennard-Jones (ULJ). The downhill barrier is 1.55 ϵ and the uphill barrier is 6.07 ϵ per supercell. The distance between the two minima is $D=1.01\,\sigma$ and the cooperativity index is $\tilde{N}=1.13$. These quantities are defined in Sec. IV C.

For illustration, the uphill and downhill barrier distributions for diffusive and nondiffusive processes for database SW3 using a threshold distance of $0.8\,\sigma$ are shown in Fig. 12. The corresponding distributions obtained for other databases are similar and are omitted for brevity. Although the distributions overlap, they peak at significantly different energies, suggesting that the ''threshold distance'' criterion is meaningful. Furthermore, the diffusive downhill barrier distribution peaks at around $0.5\,\epsilon$, corresponding to about 1 eV, in reasonable agreement with experiment.[45,46] All the rearrangements described by Barkema and Mousseau[40,42] would be classified as diffusive in this scheme, because they lead to a change in coordination.

We suggest that the PES for *a*-Si contains many relatively deep funnels, in which the intrafunnel processes are nondiffusive and fast, while the interfunnel processes are diffusive and slow. Structural relaxation takes place via interfunnel motion, with interfunnel barriers corresponding to those observed experimentally for transport properties[45,46] and found theoretically by Barkema and Mousseau.[40,42,44] The Arrhenius temperature dependence of relaxation processes in strong liquids such as *a*-Si suggests that the barrier distribution for *diffusive* processes is similar throughout the PES, which is not inconsistent with our results. However, the present multifunnel picture is different from the ''uniformly rough'' view of strong glass formers.[15]

The tetrahedrally coordinated open network structure of *a*-Si also enables nondiffusive processes to be described as relative motion of tetrahedra, whereas in diffusive processes, the coordination of tetrahedra changes. Hence there is probably a connection to the high- and low-frequency modes observed by Elliott and Taraskin.[21]

Separation of nondiffusive and diffusive rearrangements is also possible for the BLJ databases, although it is not as clear. The threshold distance criterion is also applicable.

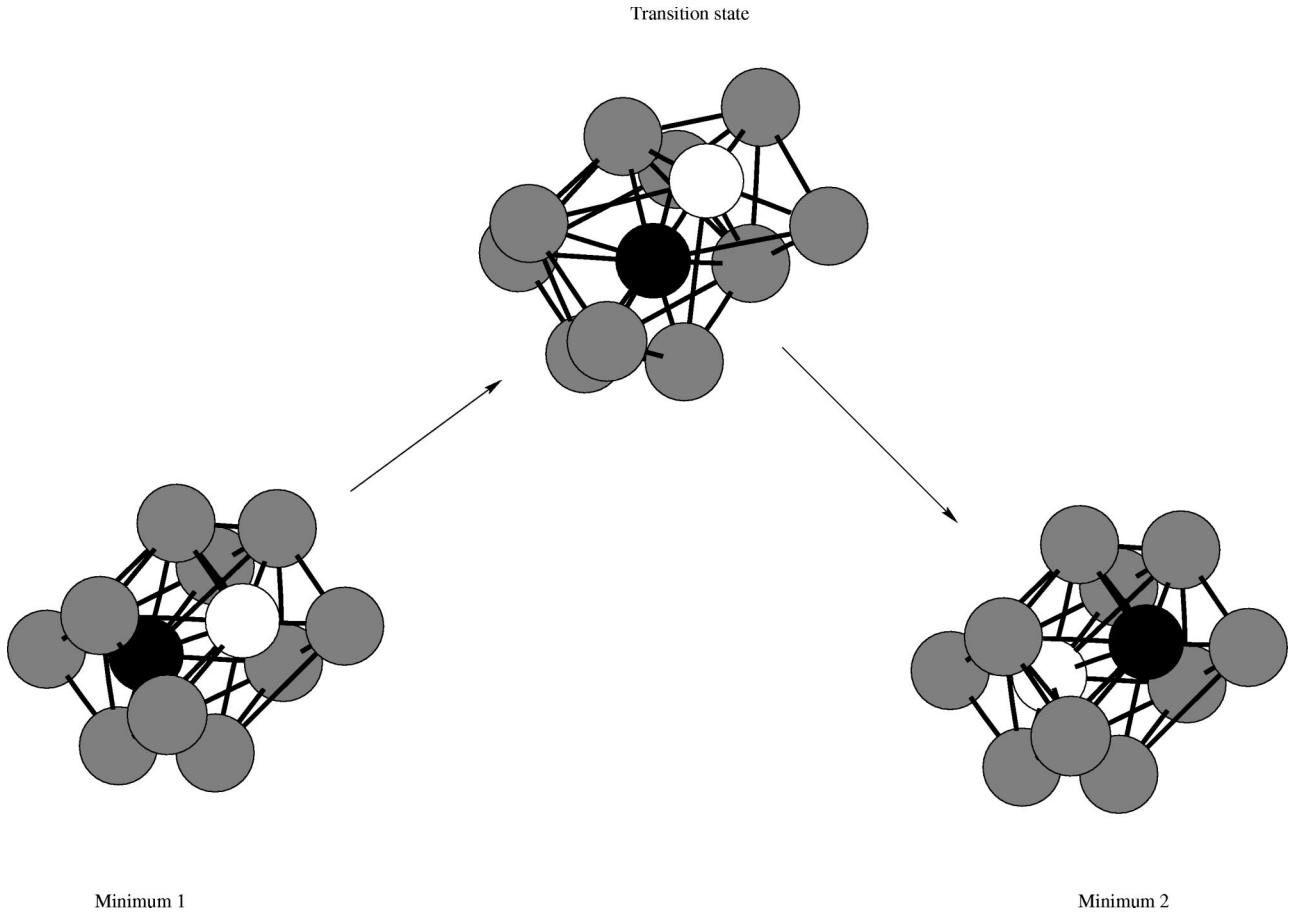

FIG. 11. Degenerate rearrangement (Ref. 95) illustrating the exchange of two atoms (shaded black and white) in unit density Lennard-Jone (ULJ). The configurations involved in this rearrangement are reasonably crystalline. The barriers are both 18.70 ϵ per supercell, the distance between the two minima is $D=1.54\,\sigma$, and the cooperativity index is $\tilde{N}=2.0$. These quantities are defined in Sec. IV C.

C. Path lengths, distances, and cooperativity indices

Features of the PES can be further characterized by the integrated path length S and the distance in configuration space D between two connected minima. The integrated path length S is estimated as a sum over steps m from the approximate steepest-descent paths:

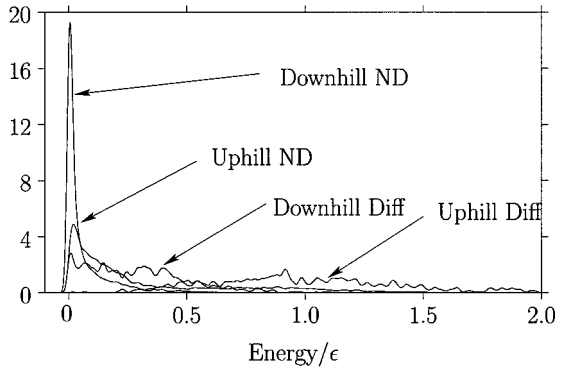

FIG. 12. Uphill and downhill barrier distributions for the Stillinger-Weber silicon database SW3, with diffusive (Diff) and nondiffusive (ND) rearrangements separated using a threshold distance of 0.8 σ. The Gaussian width $s=0.005\,\epsilon$ and the barriers are in ϵ per supercell.

$$S \approx \sum_m |\mathbf{X}(m+1)-\mathbf{X}(m)|, \tag{7}$$

where $\mathbf{X}(m)$ is the $3N$-dimensional vector of coordinates at step m. D is simply the modulus of the $3N$-dimensional vector separating the two minima in configuration space.

A measure of the localization of rearrangement i is given by the cooperativity index $\tilde{N}_i$,[103,104] defined as

$$\tilde{N}_i = \frac{\left(\sum_\alpha^N |\mathbf{r}_\alpha(s)-\mathbf{r}_\alpha(t)|^2\right)^2}{\sum_\alpha^N |\mathbf{r}_\alpha(s)-\mathbf{r}_\alpha(t)|^4}. \tag{8}$$

$\mathbf{r}_\alpha$ denotes the position vector of atom α, and s and t are the initial and final configurations in rearrangement pathway i, respectively. There seems to be little variation of S, D, and $\tilde{N}$ between the binary Lennard-Jones (BLJ) databases, except that databases BLJ1–3, generated by less extensive local searches, have slightly lower average path lengths, but in the unit density homogeneous system (ULJ) there is a striking increase in all three indices with increasing energy of the minima in the database, i.e., from ULJ1 to ULJ3, probably

owing to the increasing disorder of the samples. This result suggests that rearrangements with large path lengths, distances and cooperativity indices become more accessible as the sample becomes more disordered. We also note that databases ULJ1 and ULJ2 contain minima with significant crystallinity, so it is perhaps surprising that they do not stand out more. The only other significant trend that we have discerned is that increasing the three-body term in Stillinger-Weber silicon by 50% appears to increase the distances and path lengths between minima and decreases the cooperativity of the rearrangements.

Using a 1000-atom supercell Barkema and Mousseau[41] characterized rearrangements in amorphous silicon as highly cooperative, with typically about 50 atoms moving more than 0.1 Å. This number is larger but of a similar order to $\tilde{N}$ for representative rearrangements found in the present work for the same system using a smaller supercell.

D. Vibrational densities of states, the ''boson peak,'' and two-level systems

The geometric mean of the frequencies of the normal modes $\overline{\nu}=\Pi_{i=1}^{3N-3}(\nu_i)^{1/3N-3}$ is of interest, as it directly affects the rate of crossing of potential energy barriers:[105–108] the higher the geometric mean frequency, the faster potential barriers are crossed. Of course, $\overline{\nu}$ also affects the thermodynamics. The dependence of $\overline{\nu}$ on the energy of the minimum is illustrated in Fig. 13 for all four systems studied. The BLJ samples exhibit a marked increase in $\overline{\nu}$ with energy, in agreement with Sastry,[109] while the Stillinger-Weber systems show the opposite trend. The behavior of the homogeneous Lennard-Jones systems ULJ and RLJ is intermediate: a slight increase in $\overline{\nu}$ is visible at higher energies.

The behavior of vibrational frequencies and the degree of anharmonicity,[7,110–112] plays an important role in recent interpretation of strong/fragile behavior.[109,113] Sastry suggests that the fragile character of the BLJ system arises from the decrease of vibrational frequencies with the energy of the local minima. Hence, as the system relaxes to lower minima, the lower frequencies provide an additional reason for barrier crossing rates and transport processes to slow down.[109] Alternatively, Wales and Doye interpret the increasing free energy barrier to diffusion observed for fragile systems at lower temperature in terms of occupation of deeper kinetic traps lower down the PES.[113] Here, higher frequencies, relative to the energy scale defined by the interatomic potential, assist relaxation so that the system samples the increasing free energy barriers associated with deeper traps. Since BLJ exhibits larger reduced frequencies than SW silicon and the opposite trend for the variation of $\overline{\nu}$ with energy, these two views of how fragility might arise are not incompatible. However, some caution is needed in the interpretation of these results, as the behavior of $\overline{\nu}$ may be different for constant pressure calculations.

Within the harmonic approximation, the eigenvalues of the mass-weighted Hessian yield the normal-mode frequencies, and the components of the corresponding eigenvectors are proportional to the atomic displacements. We will focus on the eigenvalues and eigenvectors of the lowest-frequency modes, as these may be involved in the boson peak.[114,115]

The vibrational densities of states (VDOS) divided by the square of the angular frequency $g(\omega)/\omega^2$ are presented in Fig. 14 for databases of both nearly crystalline and amorphous ULJ and SW samples [databases ULJ(x), SW(x), ULJ3, and SW3, respectively]. The crystalline databases were generated using SS3 (Sec. III B). The Debye approximation treats the vibrations as sinusoidal waves in an elastic continuum, predicting that the $g(\omega)\sim\omega^2$ up to a cutoff frequency ν_D. For SW silicon, the reduced unit of frequency corresponds to 13.0 THz, and for the Lennard-Jones systems it corresponds to 0.47 THz (using parameters appropriate for argon).

A popular measure of the localization of vibrational mode j is the participation ratio p_j that is essentially N^{-1} times the inverse of the moment ratio of the atomic displacements as expressed in Eq. (8).[20–23,116] The atomic displacements for the normal modes are obtained from the eigenvectors of the Hessian matrix. p_j varies from 1 for a completely delocalised mode, in which all atoms move the same distance, to $1/N$ for a mode in which only one atom moves. $p_j=2/3$ for a sinusoidal standing wave. Several authors have found modes that are combinations of delocalized and localized components.[21–23] These contributions may have a low value of p_j, despite their partially delocalized nature, if the atomic displacements of the localized components are large.

Finite-size effects are immediately obvious for the crystals: distinct peaks are visible, and there appears to be a cutoff frequency at the low-frequency end of the band. These phenomena are due to the finite box length restricting the possible phonon wavelengths.

The VDOS and variation of participation ratios for the amorphous databases agree well with previous work[23,117] (see Fig. 15). The effect of disorder on the modes is visible as an increase in $g(\omega)/\omega^2$ in the low-frequency region. The participation ratios for the low-frequency modes suggest significant localization. We examined plots of the Cartesian components of the normal-mode displacement vectors against the projection of their positions, as used in Refs. 21 and 23, but the supercells considered in the present work contain too few atoms for a distinct sinusoidal component to be visible. However, localized random components are present.

If two-level systems (TLS) and the boson peak are produced by the same soft, anharmonic modes, one would expect it to be possible to verify this connection using eigenvector following.[62–68] A good candidate for a TLS was found in database SW2, although such features are apparently experimentally absent in annealed a-Si.[34] We investigated further using eigenvector-following transition state searches from one of the corresponding minima. Some adjustment of the parameters in the transition state search was required, as the PES is very flat: small step lengths ($0.005\,\sigma$) and push-offs ($0.001\,\sigma$) were needed to prevent the optimization from overshooting. Minimization was carried out using the Page and McIver steepest-descent method, with analytic first and second derivatives,[118] to ensure that the correct minima were found. A number of new pathways were found, all with low

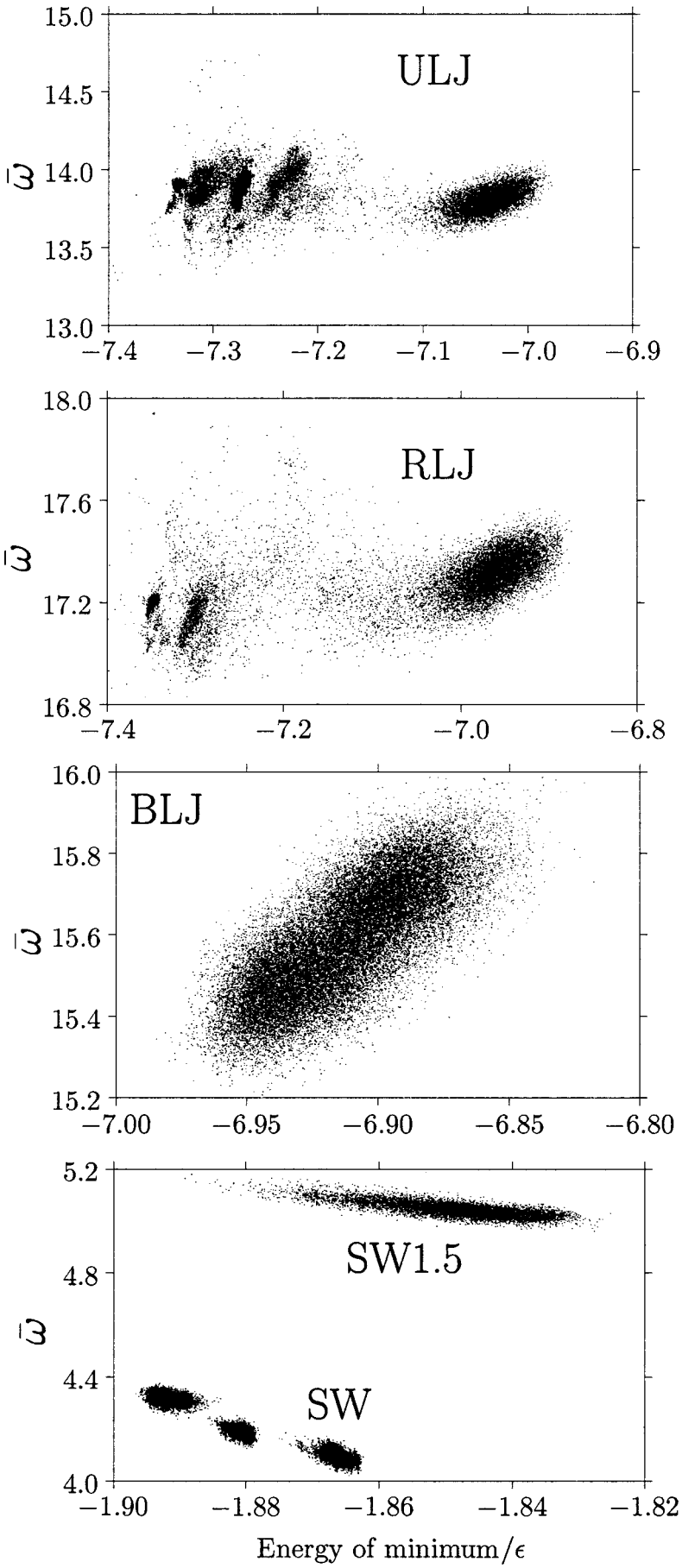

FIG. 13. Scatter plot of geometric mean normal-mode frequency $\bar{\omega}=2\pi\bar{\nu}$ in reduced units against the energy per atom of the corresponding minimum in ϵ (ϵ_{AA} for BLJ). Samples ULJ1, ULJ2, and RLJ1 contain numerous minima with significant crystalline character, which correspond to the features at lower energy in the ULJ and RLJ panels.

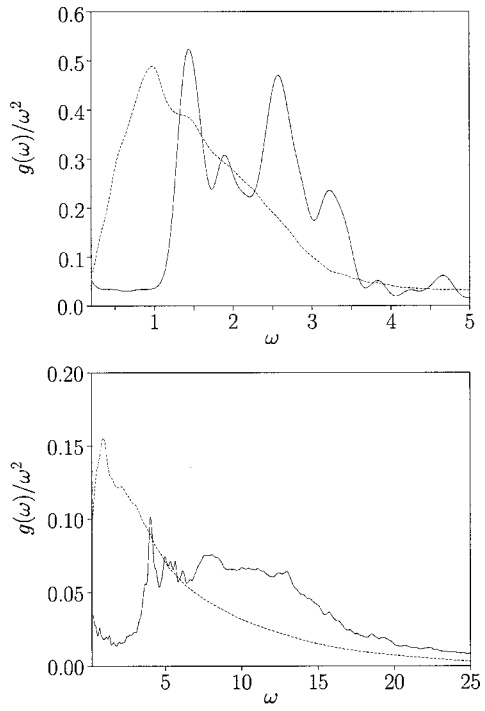

FIG. 14. Normalized vibrational densities of states (VDOS) divided by frequency squared $[g(\omega)/\omega^2$, in units of $(m\sigma^2/\epsilon)^{3/2}]$ as a function of ω (in units of $\sqrt{\epsilon/m\sigma^2}$) for databases SW3 (top) and ULJ3 (bottom) (dotted lines) compared with those for crystalline databases of minima (solid lines).

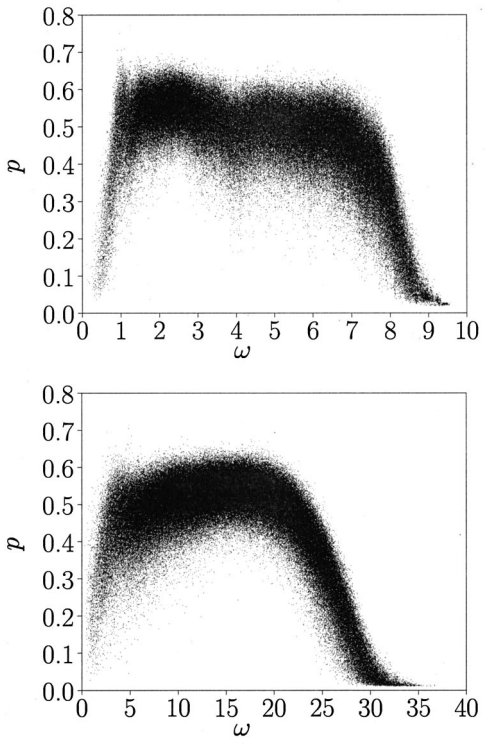

FIG. 15. Plot of participation ratio p against frequency (in units of $\sqrt{\epsilon/m\sigma^2}$) for databases SW3 (top panel) and ULJ3 (bottom panel). p is defined in Sec. IV D.

barriers (Table III). Of particular interest is the pathway with an uphill barrier corresponding to 5.28 K (per supercell) and a downhill barrier of 5.14 K per supercell, as it has an asymmetry of 0.14 K per supercell. Such results provide some evidence to support Angell's hypothesis that the low-frequency modes and two-level systems are related.

V. CONCLUSIONS

The classification of rearrangements as diffusive or nondiffusive reveals a significant difference between the ''strong'' system (SW silicon) and the ''fragile'' systems (Lennard-Jones). For all the pathways that we have visualized, diffusive and nondiffusive processes can be separated by determining whether any atoms move more than a threshold distance between the connected minima. In reality there must be a continuum of mechanisms between the ''diffusive'' and ''nondiffusive'' limits, and the distance criterion is simply a means to gain further insight into properties of the potential energy surface.

In the LJ systems the diffusive rearrangements generally have barriers about one order of magnitude greater than the nondiffusive, while for SW silicon the barriers corresponding to the two types of rearrangement differ by about three orders of magnitude. This observation, if it can be generalized, leads us to suggest a deeper multifunnel character for the energy landscapes of strong glass formers, in contrast to the ''uniformly rough'' picture.[15] However, if we coarse grain by averaging over the fast processes that do not contribute to diffusion then the ''uniformly rough'' view may be recovered. In this picture the nondiffusive processes in strong glass formers will be fast, while the α processes may not be seen in dielectric relaxation experiments because they are frozen out. The effective barriers to transport dynamics such as diffusion are those for the interfunnel α processes, that correspond to a number of elementary rearrangements, in accord with Stillinger's suggestion.[15] Experiment suggests that these effective barriers do not vary significantly throughout the PES, in agreement with our results, as relaxation processes tend to have Arrhenius temperature dependence in ''strong'' liquids. In the model fragile liquids considered in the present work, the distinction between diffusive and nondiffusive processes is much less pronounced than in the strong systems. The energy landscape may therefore have shallower funnels, and this feature may contribute to non-Arrhenius behavior and stretched exponential relaxation.

In fact, none of our barrier height distributions show much variation with the average energy of the local minima involved, a result that highlights the importance of the actual connectivity of the PES for dynamics. The ubiquitous presence of low barrier ''nondiffusive'' rearrangements also implies that the system is not trapped in a single local minimum below the glass transition temperature. Hence, the configurational entropy does not vanish at T_g; instead we would expect the freezing out of diffusive rearrangements on the experimental time scale to limit the accessible minima to one of the subsets that are connected by only ''nondiffusive'' mechanisms. This picture has been incorporated in our recent energy landscape model of glasses.[113]

TABLE III. Characteristics of five rearrangements from sample SW2 where the minima are possible candidates for two-level systems (TLS). We tabulate the energy of the transition state, the downhill barrier, the difference in energy ΔE in ϵ and K, the path length S, and the distance D between the pairs of minima (see Sec. IV C).

Energy per atom	Downhill barrier/$10^{-6}\,\epsilon$	$\Delta E/10^{-6}\,\epsilon$	ΔE/K	S	D
−1.8785	139.245	1.824	0.045	0.114	0.107
−1.8806	204.286	5.4884	0.138	0.128	0.124
−1.8800	5.333	7.9904	0.201	0.057	0.057
−1.8797	18.713	20.9291	0.527	0.064	0.063
−1.8833	0.120	43.0708	1.083	0.055	0.054

The trends that we have observed for the normal-mode frequencies are also in line with recent interpretation of strong/fragile behavior.[109,113] The decreasing frequencies found for lower-energy minima in BLJ will slow down barrier crossing as temperature decreases[109] and may therefore contribute to fragile behavior. It is noteworthy that the frequencies found in the SW silicon samples exhibit the opposite behavior. The reduced frequencies of all the Lennard-Jones systems are also significantly larger than for SW silicon. This observation fits with the suggestion that higher frequencies enable the system to occupy deeper kinetic traps on a given time scale, and hence access increasing free energy barriers and exhibit more fragile behavior.[113] Higher frequencies are also associated with a larger number of local minima,[8,113] which is consistent with the thermodynamic properties exhibited by fragile glass formers.[113] The unit density (negative pressure) and relaxed (zero pressure for the crystal) Lennard-Jones systems also enable us to interpret the effect of pressure on fragility. As expected, the relaxed Lennard-Jones system exhibits significantly higher frequencies. Increasing the pressure should reduce the number of local minima on the PES.[9,10] However, the higher frequencies would enable the system to reach deeper regions of the PES and sample larger free energy barriers. Experimental results for silica show that this archetypal strong system exhibits dynamical fragility at high pressure,[7] in agreement with the above theory. However, the same theory would predict that systems under pressure will exhibit a smaller heat-capacity difference between liquid and glass, and might therefore appear thermodynamically stronger.

The minima that we have found exhibit the increased low-frequency VDOS expected for disordered systems, and we have characterized several candidate two-level systems for SW silicon. The eigenvector-following approach should be able to clarify the relationship of soft vibrational modes to low-lying transition states. The preliminary results presented here suggest that the softest normal modes of minima in candidate two-level systems may well be connected to low-energy transition states. Disconnectivity graphs for the low-energy regions of two databases containing minima dominated by crystalline order reveal a ''palm-tree'' structure, indicating that crystallization can proceed rapidly once a critical nucleus has formed.

ACKNOWLEDGMENTS

We acknowledge fruitful discussions with Dr. S. N. Taraskin and Professor S. R. Elliott about the boson peak and related phenomena. We are also grateful to Dr. M. A. Miller and P. N. Mortenson for their help with certain programs and to Dr. J. P. K. Doye for numerous discussions. Dr. R. Malek and Dr. N. Mousseau kindly provided the coordinates of the Lennard-Jones minima used as starting points in Ref. 73. D. J. W. and T. F. M. are grateful to the Royal Society and the EPSRC for financial support, respectively.

APPENDIX A: FURTHER DETAILS OF TRANSITION STATE SEARCHES

A new strategy was adopted to locate as many different transition states as possible for a given minimum and a fixed number of searches. A random search direction is chosen, as in the ART approach.[40–44,73] Instead of displacing the system in steps until a negative curvature is first encountered we assume that the motion will be limited by the first collision. Using standard code for the simulation of hard-sphere dynamics,[119] and interpreting a $3N$-dimensional vector of uniform random numbers as components of the velocity vector, we calculate the time of the first hard-sphere collision τ. The hard-sphere radius is set equal to half the equilibrium pair separation for the potential in question ($2^{1/6}\sigma_{AA}$ was used for BLJ). We considered the effect of starting the EF/BFGS hybrid eigenvector-following approach from the configuration advanced to a time of either $\tau/2$ or τ and found that using the full collision time was most effective in each test. If there were no interatomic potential then we could follow a ''colliding'' pair of atoms further in time to the point where their separation is again equal to the equilibrium pair separation τ'. We also considered transition state searches starting from the configuration obtained at time $(\tau+\tau')/2$, with the distance between the two colliding atoms renormalized to the equilibrium pair separation.

The results for 3000 searches started from clusters of 13, 38, and 55 atoms bound by the Lennard-Jones potential are shown in Table IV and compared with the statistics reported by Malek and Mousseau[73] for the same minima. The total number of transition states and the number directly connected to the starting minimum always increases in the same order. However, the number of unconnected transition states and minima, which cannot reach the starting minimum via any sequence of rearrangements within the set generated, also increases. Only globally connected databases of minima can be used to construct disconnectivity graphs (Sec. III D)

TABLE IV. Results of 3000 transition state searches for the three Lennard-Jones clusters studied using the ART approach in Ref. 73. Statistics were obtained for starting points corresponding to displacements of half and the full hard-sphere first collision time τ, as well as for the adjusted configuration at time $(\tau+\tau')/2$, as described in Appendix A. In each case we report the total number of different transition states and new minima obtained, i.e., permutational isomers are not counted. For the transition states the first number in brackets is the number that is directly connected to the starting minimum in question, and the second number is the number that is not connected to the starting minimum by any series of rearrangements within the set of stationary points obtained. For the minima the number in brackets is the number that is not connected to the starting minimum by any series of rearrangements within the set of stationary points. For example, using $\tau/2$ for LJ_{13} we see that 130 transition states and 65 new minima were found. 60 of the new minima are directly connected to the original minimum, and therefore five are not. However, the latter five minima can reach the starting minimum via transition states and minima within the connected set.

Cluster		ART (Ref. 73)	$\tau/2$	τ	$(\tau+\tau')/2$
LJ_{13}	transition states	72	130 (60,0)	160 (65,0)	606 (113,9)
	new minima	44	65 (0)	82 (0)	238 (14)
LJ_{38}	transition states	109	162 (86,22)	179 (95,9)	1694 (256,741)
	new minima	73	168 (40)	175 (18)	2188 (1376)
LJ_{55}	transition states	151	217 (152,9)	316 (201,24)	1166 (398,251)
	new minima	89	183 (17)	271 (47)	1094 (489)

or for master-equation dynamics simulations, and we therefore discarded all the unconnected stationary points that were generated. For all the databases reported in the present work, except SW3, we started transition state searches from configurations corresponding to the first collision time τ. From Table IV it might appear that the adjusted configuration at time $(\tau+\tau')/2$ would be more efficient, but for the present bulk systems this larger initial perturbation led to an undesirable number of disconnected transition states, except for sample SW3.

APPENDIX B: STARTING MINIMA FOR SW, ULJ, AND RLJ

To generate starting minima for the Stillinger-Weber and the unit density (ULJ) and relaxed (RLJ) Lennard-Jones systems we first conducted standard MD runs of increasing total energy starting from the appropriate crystal. Quenches were performed at regular intervals to determine when the (superheated) system first escaped from the crystal. The quench minima following escape were each used as the starting points for exploration of the PES using the SS3 sampling scheme (Sec. III B). We found that initial minima containing even small regions of crystallinity collapsed to the crystal after a few hundred minima (or less) had been sampled. However, eventually a starting minimum was always located where the crystal was not found in the SS3 procedure even after sampling several thousand minima. The starting minima used in the generation of the final databases were chosen from these intermediate databases that did not collapse to the crystal. The intermediate databases were then discarded.

Databases SW1–3 were generated using SS2 (Sec. III B) starting from minima at the bottom, middle, and top of the intermediate SS3 database, respectively, in terms of their energy. Database SW1.5 was generated using SS2 starting from the same minimum as for SW1, but reoptimized with the new potential. Databases ULJ1–3 were generated using SS2 starting from minima at the bottom, middle, and top of the intermediate SS3 databases, as for SW1–3. Databases RLJ1 and RLJ2 were generated using SS2 starting from minima at the bottom and top of the intermediate SS3 database.

Although the intermediate SS3 database for ULJ did not collapse to the crystal, it nevertheless managed to reach minima containing significant crystalline character. The starting configurations for the ULJ1 and ULJ2 databases appear to be by inspection about 80% and 50% crystalline, respectively, although the average value of the crystallinity order parameter Q_6 is similar. However, their barrier distributions are not very different from ULJ3. All the other starting minima and the corresponding databases, including ULJ3, have no discernible crystalline character.

[1] M. Goldstein, J. Chem. Phys. **51**, 3728 (1969).
[2] W. Götze, in *Liquids, Freezing and the Glass Transition, Les Houches, Session LI, 1989*, edited by J.-P. Hansen, D. Levesque, and J. Zinn-Justin (North-Holland, Amsterdam, 1991), pp. 287–499.
[3] G. Fulcher, J. Am. Ceram. Soc. **8**, 339 (1925).
[4] H. Vogel, Z. Phys. **22**, 645 (1921).
[5] G. Tammann and W. Hesse, Z. Anorg. Allg. Chem. **156**, 245 (1926).
[6] C.A. Angell, J. Non-Cryst. Solids **131-133**, 13 (1991).
[7] C.A. Angell, Science **267**, 1924 (1995).
[8] D.J. Wales, J.P.K. Doye, M.A. Miller, P.N. Mortenson, and T.R. Walsh, Adv. Chem. Phys. **115**, 1 (2000).
[9] D.J. Lacks, Phys. Rev. Lett. **80**, 5385 (1998).

[10] D.L. Malandro and D.J. Lacks, J. Chem. Phys. **107**, 5804 (1997).
[11] W. Kauzmann, Chem. Rev. **43**, 219 (1948).
[12] G. Williams and D. Watts, J. Chem. Soc., Faraday Trans. **66**, 80 (1970).
[13] R.G. Palmer, D.L. Stein, E. Abrahams, and P.W. Anderson, Phys. Rev. Lett. **53**, 958 (1984).
[14] G.P. Johari and M. Goldstein, J. Chem. Phys. **53**, 2372 (1970).
[15] F.H. Stillinger, Science **267**, 1935 (1995).
[16] P. Leopold, M. Montal, and J. Onuchic, Proc. Natl. Acad. Sci. U.S.A. **89**, 8721 (1992).
[17] J. Doye, M. Miller, and D. Wales, J. Chem. Phys. **111**, 8417 (1999).
[18] U. Buchenau, N. Prager, N. Nücker, A. Dianoux, N. Ahmad, and W. Phillips, Phys. Rev. B **34**, 5665 (1986).
[19] A. Sokolov, E. Rossler, A. Kisliuk, and D. Quitmann, Phys. Rev. Lett. **71**, 2062 (1993).
[20] S. Taraskin and S. Elliott, Europhys. Lett. **39**, 37 (1997).
[21] S.N. Taraskin and S.R. Elliot, Phys. Rev. B **59**, 8572 (1999).
[22] H. Schober and C. Oligschleger, Phys. Rev. B **53**, 11 469 (1996).
[23] V. Mazzacurati, G. Ruocco, and M. Sampoli, Europhys. Lett. **34**, 681 (1996).
[24] T. Uchino and T. Yoko, J. Chem. Phys. **108**, 8130 (1998).
[25] G. Guillot and Y. Guissani, Phys. Rev. Lett. **78**, 2401 (1997).
[26] S.D. Bembenek and B.B. Laird, Phys. Rev. Lett. **74**, 936 (1995).
[27] S.P. Das, Phys. Rev. E **59**, 3870 (1999).
[28] P. Anderson, B. Halperin, and C. Varma, Philos. Mag. **25**, 1 (1972).
[29] W. Phillips, J. Low Temp. Phys. **7**, 351 (1972).
[30] R. Zeller and R. Pohl, Phys. Rev. B **4**, 2029 (1971).
[31] G. Daldoss, O. Pilla, G. Viliani, and C. Brangian, Phys. Rev. B **60**, 3200 (1999).
[32] C.A. Angell and C.T. Moynihan, Metall. Mater. Trans. B **31B**, 4587 (2000).
[33] N.I. Agladze and A.J. Sievers, Phys. Rev. Lett. **80**, 4209 (1998).
[34] X. Liu, B. White, R. Pohl, E. Iwanizcko, K.M. Jones, A.H. Mahan, B. Nelson, R.S. Crandall, and S. Veprek, Phys. Rev. Lett. **78**, 4418 (1997).
[35] F.H. Stillinger and T.A. Weber, Phys. Rev. A **25**, 978 (1982).
[36] F.H. Stillinger and T.A. Weber, Phys. Rev. A **28**, 2408 (1983).
[37] H. Jonsson and H.C. Andersen, Phys. Rev. Lett. **60**, 2295 (1988).
[38] S. Sastry, P.G. Debenedetti, and F.H. Stillinger, Nature (London) **393**, 554 (1998).
[39] G. Barkema and N. Mousseau, Phys. Rev. Lett. **77**, 4358 (1996).
[40] G. Barkema and N. Mousseau, Phys. Rev. Lett. **81**, 1865 (1998).
[41] G.T. Barkema and N. Mousseau, Phys. Rev. B **62**, 4985 (2000).
[42] N. Mousseau and G.T. Barkema, Phys. Rev. B **61**, 1898 (2000).
[43] G. Barkema, N. Mousseau, and S. de Leeuw, J. Chem. Phys. **112**, 960 (2000).
[44] G. Barkema and N. Mousseau, Comput. Phys. Commun. **122**, 206 (1999).
[45] J. Shin and H. Atwater, Phys. Rev. B **48**, 5964 (1993).
[46] S. Roorda, W. Sinke, J. Poate, D. Jacobson, S. Dierker, B. Dennis, D. Eaglesham, F. Spaepen, and P. Fuoss, Phys. Rev. B **44**, 3702 (1991).
[47] A. Heuer, Phys. Rev. Lett. **78**, 4051 (1997).
[48] L. Angelani, G. Parisi, G. Ruocco, and G. Viliani, Phys. Rev. Lett. **81**, 4648 (1998).
[49] L. Angelani, G. Parisi, G. Ruocco, and G. Viliani, Phys. Rev. E **61**, 1681 (2000).
[50] S. Büchner and A. Heuer, Phys. Rev. Lett. **84**, 2168 (2000).
[51] P. Chaudhury and S.P. Bhattacharyya, Int. J. Quantum Chem. **76**, 161 (2000).
[52] J.E. Jones and A.E. Ingham, Proc. R. Soc. London, Ser. A **107**, 636 (1925).
[53] F.H. Stillinger and T.A. Weber, Phys. Rev. B **31**, 1954 (1985).
[54] W. Kob and J.-L. Barrat, Phys. Rev. Lett. **78**, 4581 (1997).
[55] W. Kob and J.-L. Barrat, Physica A **263**, 234 (1999).
[56] W. Kob and H. Andersen, Phys. Rev. E **51**, 4626 (1995).
[57] F.H. Stillinger and T.A. Weber, Phys. Rev. B **31**, 5262 (1985)
[58] H. Andersen and K. Ding, Phys. Rev. B **34**, 6987 (1986).
[59] F.H. Stillinger and T.A. Weber, Science **225**, 983 (1984).
[60] C.J. Tsai and K.D. Jordan, J. Phys. Chem. **97**, 11 227 (1993).
[61] F.H. Stillinger, Phys. Rev. E **59**, 48 (1999).
[62] G.M. Crippen and H.A. Scheraga, Arch. Biochem. Biophys. **144**, 462 (1971).
[63] J. Pancíř, Collect. Czech. Chem. Commun. **40**, 1112 (1974).
[64] R.L. Hilderbrandt, Comput. Chem. (Oxford) **1**, 179 (1977).
[65] C. Cerjan and W. Miller, J. Chem. Phys. **75**, 2800 (1981).
[66] D. Wales, J. Chem. Phys. **101**, 3750 (1994).
[67] D. Wales and T. Walsh, J. Chem. Phys. **105**, 6957 (1996).
[68] L. Munro and D. Wales, Phys. Rev. B **59**, 3969 (1999).
[69] D. Wales, J. Chem. Phys. **91**, 7002 (1989).
[70] D. Wales, Chem. Phys. Lett. **166**, 419 (1990).
[71] D. Liu and J. Nocedal, Math. Program. **45**, 503 (1989).
[72] W. Press, B. Flannery, S. Teukolsky, and W. Vetterling, *Numerical Recipes* (Cambridge University Press, Cambridge, England, 1986).
[73] R. Malek and N. Mousseau, Phys. Rev. E **62**, 7723 (2000).
[74] C. Tsai and K. Jordan, J. Phys. Chem. **97**, 11 227 (1993).
[75] J.P.K. Doye and D.J. Wales, Z. Phys. D: At., Mol. Clusters **40**, 194 (1997).
[76] N. Mousseau and G. Barkema, Phys. Rev. E **57**, 2419 (1998).
[77] H.E.A. Huitema, J.P. van der Eerden, J.J.M. Janssen, and H. Human, Phys. Rev. B **62**, 14 690 (2000).
[78] C. Angell, B. Richards, and V. Velikov, J. Phys.: Condens. Matter **11**, A75 (1999).
[79] F. Sciortino, W. Kob, and P. Tartaglia, Phys. Rev. Lett. **83**, 3214 (1999).
[80] T.B. Schroder, S. Sastry, J.C. Dyre, and S.C. Glotzer, J. Chem. Phys. **112**, 9834 (2000).
[81] C. Donati, F. Sciortino, and P. Tartaglia, Phys. Rev. Lett. **85**, 1464 (2000).
[82] S. Sastry, Phys. Rev. Lett. **85**, 590 (2000).
[83] S. Sastry, J. Phys.: Condens. Matter **12**, 6515 (2000).
[84] F. Sciortino, W. Kob, and P. Tartaglia, J. Phys.: Condens. Matter **12**, 6525 (2000).
[85] L. Angelani, R. Di Leonardo, G. Ruocco, A. Scala, and F. Sciortino, Phys. Rev. Lett. **85**, 5356 (2000).
[86] K. Broderix, K.K. Bhattacharya, A. Cavagna, A. Zippelius, and I. Giardina, Phys. Rev. Lett. **85**, 5360 (2000).
[87] D. Wales and J. Doye, J. Phys. Chem. A **101**, 5111 (1997).
[88] D.J. Wales and H.A. Scheraga, Science **285**, 1368 (1999).
[89] P. Steinhardt, D. Nelson, and M. Ronchetti, Phys. Rev. B **281**, 784 (1983).
[90] R.M. Lynden-Bell and D.J. Wales, J. Chem. Phys. **101**, 1460 (1994).
[91] O.M. Becker and M. Karplus, J. Chem. Phys. **106**, 1495 (1997).

[92] D. Wales, M. Miller, and T. Walsh, Nature (London) **394**, 758 (1998).
[93] K.M. Westerberg and C.A. Floudas, J. Chem. Phys. **110**, 9259 (1999).
[94] P. Garstecki, T.X. Hoang, and M. Cieplak, Phys. Rev. E **60**, 3219 (1999).
[95] R.E. Leone and P.v.R. Schleyer, Angew. Chem. Int. Ed. Engl. **9**, 860 (1970).
[96] N.P. Kopsias and D.N. Theodorou, J. Chem. Phys. **109**, 8573 (1998).
[97] R.S. Berry and R. Breitengraser-Kunz, Phys. Rev. Lett. **74**, 3951 (1995).
[98] R.E. Kunz and R.S. Berry, J. Chem. Phys. **103**, 1904 (1995).
[99] D. Donati, J. Douglas, W. Kob, S. Plompton, P. Poole, and S. Glotzer, Phys. Rev. Lett. **80**, 2338 (1998).
[100] B. Doliwa and A. Heuer, Phys. Rev. Lett. **80**, 4915 (1998).
[101] D.J. Wales and J. Uppenbrink, Phys. Rev. B **50**, 12 342 (1994).
[102] L.J. Munro and D.J. Wales, Faraday Discuss. **106**, 409 (1997).
[103] M.A. Miller, J. Doye, and D. Wales, J. Chem. Phys. **110**, 328 (1999).
[104] F.H. Stillinger and T.A. Weber, J. Phys. Chem. **87**, 2833 (1983).
[105] O.K. Rice and H.C. Ramsperger, J. Am. Chem. Soc. **49**, 1617 (1927).
[106] L.S. Kassel, J. Phys. Chem. **32**, 225 (1928).
[107] R.A. Marcus and O.K. Rice, J. Phys. Colloid Chem. **55**, 894 (1951).
[108] R. G. Gilbert and S. C. Smith, *Theory of Unimolecular and Recombination Reactions* (Blackwell, Oxford, 1990).
[109] S. Sastry, Nature (London) **409**, 164 (2001).
[110] G.P. Johari, Philos. Mag. B **41**, 41 (1981).
[111] A.P. Sokolov, A. Kisliuk, M. Soltwisch, and D. Quitmann, Phys. Rev. Lett. **69**, 1540 (1992).
[112] C.A. Angell, J. Phys.: Condens. Matter **12**, 6463 (2000).
[113] D.J. Wales and J.P.K. Doye, Phys. Rev. B **63**, 214204 (2001).
[114] U. Buchenau, Y. Galperin, V. Gurevich, and H. Schober, Phys. Rev. B **43**, 5039 (1991).
[115] U. Buchenau, Y. Galperin, V. Gurevich, D. Parshin, M. Ramos, and H. Schober, Phys. Rev. B **46**, 2798 (1992).
[116] R. Bell and P. Dean, Philos. Mag. **25**, 1381 (1972).
[117] S. Taraskin (unpublished).
[118] M. Page and J.W. McIver, J. Chem. Phys. **88**, 922 (1988).
[119] M. P. Allen and D. J. Tildesley, *The Computer Simulation of Liquids* (Clarendon Press, Oxford, 1987).
[120] S.D. Stoddard and J. Ford, Phys. Rev. A **8**, 1504 (1973).